Exit of spore dormancy transforms the yeast cytoplasm and the solubility of its proteome

Samuel Plante[1,2,3,4,5], Kyung-Mee Moon[6], Pascale Lemieux[1,2,3,4,5], Leonard J. Foster[6], and Christian R. Landry[1,2,3,4,5]

Affiliations

[1]Institut de Biologie Intégrative et des Systèmes (IBIS), 1030, avenue de la Médecine, Université Laval, Québec (Québec), Canada, G1V 0A6

[2]Regroupement Québécois de Recherche sur la Fonction, l'Ingénierie et les Applications des Protéines, (PROTEO), 1045 Avenue de la Médecine, Université Laval, Québec (Québec), Canada, G1V 0A6

[3]Département de biologie, 1045 Avenue de la Médecine, Université Laval, Québec (Québec), Canada, G1V 0A6.

[4]Département de biochimie, microbiologie et bio-informatique, 1045 Avenue de la Médecine, Université Laval, Québec (Québec), Canada, G1V 0A6.

[5]Centre de recherche en données massives (CRDM), 1065, avenue de la Médecine, Université Laval, Québec (Québec), Canada, G1V 0A6

[6]Department of Biochemistry & Molecular Biology, and Michael Smith Laboratories, University of British Columbia, Vancouver, BC, Canada, V6T 1Z4

Corresponding author:

Christian R. Landry (christian.landry@bio.ulaval.ca)
Pavillon Charles-Eugène-Marchand
1030, Avenue de la Médecine
Université Laval
Québec (Québec) G1V 0A6
Canada

Abstract

The biophysical properties of the cytoplasm are major determinants of key cellular processes and adaptation. Yeasts produce dormant spores that can withstand extreme conditions. We show that spores exhibit extraordinary biophysical properties, including a highly viscous and acidic cytosol. These conditions alter the solubility of more than 100 proteins such as metabolic enzymes that become more soluble as spores transit to active cell proliferation upon nutrient repletion. A key regulator of this transition is the heat shock protein Hsp42, which shows transient solubilization and phosphorylation, and is essential for the transformation of the cytoplasm during germination. Germinating spores therefore return to growth through the dissolution of protein assemblies, orchestrated in part by Hsp42 activity. The modulation of spores' molecular properties are likely key adaptive features of their exceptional survival capacities.

Keywords: cytoplasm, cell dormancy, protein solubility, protein phosphorylation

Graphical abstract

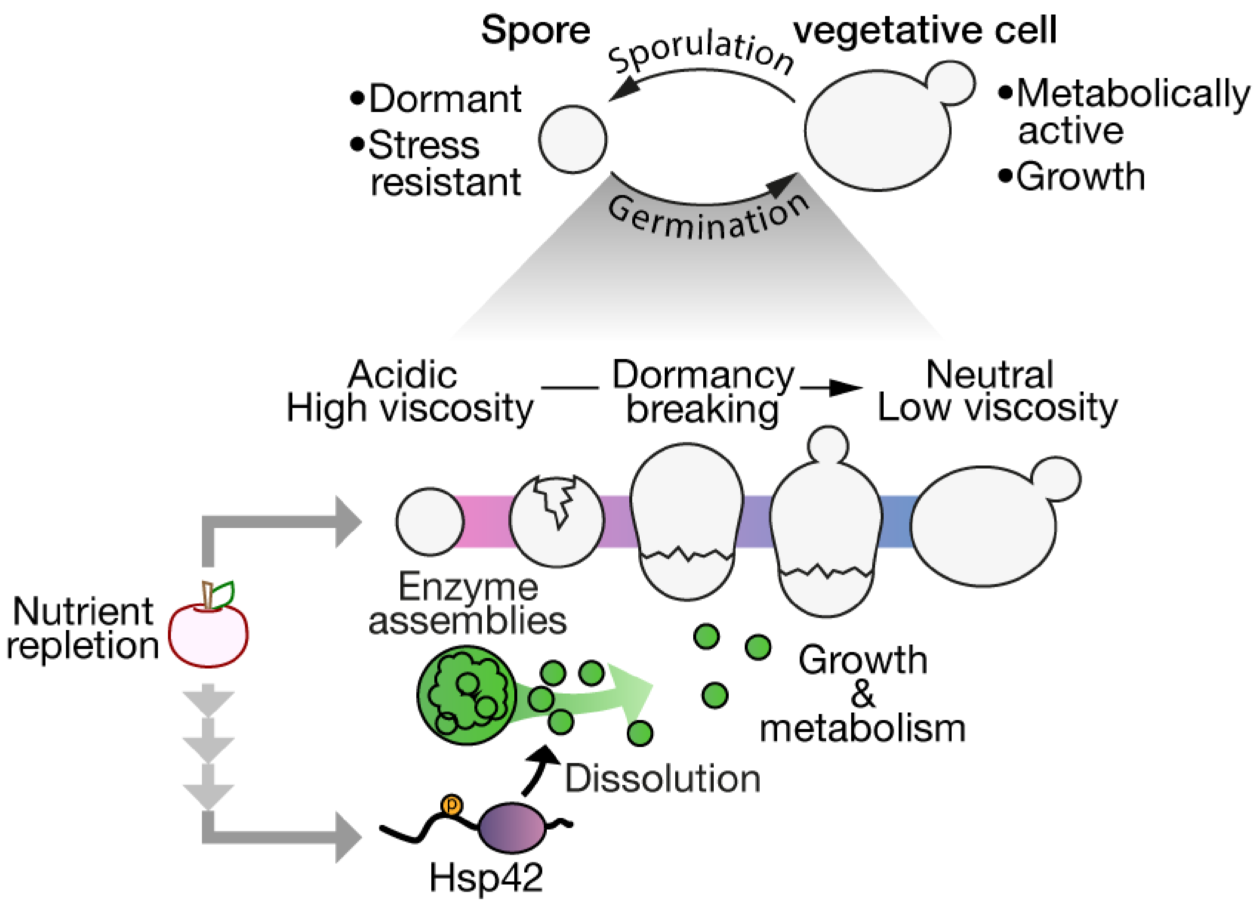

Highlights

Yeast spores are dormant cells that can withstand extreme environmental conditions

Spore cytoplasm is more dense, viscous and acidic than that of vegetative cells

Hundreds of proteins change solubility during spore activation

Hsp42 plays key role in the biophysical transformation of the spore cytoplasm

Introduction

Organisms across the tree of life rely on dormancy to withstand hostile conditions. This cellular state implies an arrest of the cell cycle and of cell metabolism, and changes in cell properties that favor survival under unfavorable conditions (Gremer and Sala, 2013; Miller et al., 2021). For instance, nematodes, rotifers and tardigrades produce dormant life-stages that allow them to resist acute stresses such as freezing, desiccation and heat stresses (García-Roger et al., 2019; Guidetti et al., 2011; Vlaar et al., 2021). In flowering plants, the embryo develops as a dormant seed, which contributes to its survival over a long period of time by resisting drought and mechanical stress until it reaches favorable conditions to resume growth (Penfield, 2017). Cell dormancy is also an adaptive strategy in cancer cells, whereby metastatic cells become dormant after dissemination and resume proliferation after treatment has succeeded at eliminating the primary tumours (Phan and Croucher, 2020). As one of the most widespread adaptive survival strategies to extreme conditions, understanding the molecular and cellular bases of cell dormancy is a major goal in cell biology.

Fungal life cycles include the production of spores. Because dormant spores are quiescent and are resistant to numerous extreme conditions such as heat, desiccation (Ho and Miller, 1978) and many harsh ecological conditions such as insect guts (Coluccio et al., 2008), sporulation is thought to be an adaptive strategy to survive changing environmental conditions (Huang and Hull, 2017). Spore stress resistance is largely attributed to the thick cell wall of specific composition (Neiman, 2011), and to the accumulation of protective compounds like trehalose or mannitol (Kane and Roth, 1974; Wyatt et al., 2013). These protective features develop during sporulation, which is typically induced by nutrient stress. When spores are exposed to favorable conditions, germination coordinates the dormancy breaking and the loss of these protective features, with cell-cycle progression and vegetative growth resumption. This transition involves multiple changes in cellular state (Herman and Rine, 1997), including the reactivation of multiple metabolic reactions. Although the precise nutrient stimuli that drive germination is dependent on ecological contexts, a carbon source such as glucose is typically an essential signal (Plante and Landry, 2020a).

Recent studies have shown the potential complex influence of the physical properties and organization of the cytosol in dormancy and stress resistance. Cytosol's viscosity, pH, crowding and protein phase separation have been linked to global cell adaptation across taxonomic groups. For instance, in tardigrades, desiccation resistance is mediated by intrinsically disordered proteins that form vitrified structures (Boothby et al., 2017). Seeds of the plant *Arabidopsis thaliana* sense hydration as the key trigger for their germination through phase separation of the protein Floe1 (Dorone et al., 2021). This process is a highly responsive environmental sensor since the biophysical state of Floe1 changes within minutes when water content is altered (Penfield, 2021). Examples of the responsiveness of the biophysics of the cell cytoplasm also come from yeast responding to acute stresses. Early heat shock response in yeast includes cytoplasm acidification (Triandafillou et al., 2020), viscosity adaptation (Persson et al., 2020), and protein phase separation (Iserman et al., 2020; Riback et al., 2017; Wallace et al., 2015). Heat shock response induces expression of many heat shock proteins composed mainly of molecular chaperones (Parsell and Lindquist, 1993) which act as a dispersal system for the heat-induced phase-separated protein condensates that promotes the rapid recovery from stress (Yoo et al., 2022).

Given that yeast spores are inherently resistant to stresses that are known to modify many biophysical features of the yeast cytoplasm, we hypothesize that the spore cytoplasm has biophysical properties similar to cells exposed to acute stress and that these will dynamically change during early spore germination. Here, we therefore examine the biophysical properties of dormant yeast spores and the changes that occur during dormancy breaking in spores of the budding yeast to unveil the molecular processes which support this critical life-history cell transition. Our results reveal that dormant spore cytosol is highly viscous and acidic, and that breaking of dormancy is supported by the neutralization and decrease in viscosity of cytoplasm. We used mass spectrometry to examine and perform proteome wide measurements of protein solubility through germination. The measurements of 895 proteins revealed dynamic changes in protein solubility through germination. We uncovered, for instance, the solubilization of several metabolic enzymes during this transition. Our results demonstrate that spores have exceptional biophysical properties and that many of the changes taking place in the cell mimic what occurs in vegetative cells experiencing stress relief. One major similarity is the implication of a small heat shock protein, Hsp42, which is essential for normal spore activation and whose activity is regulated by its phosphorylation.

Results and discussion

Spores have a dense cytoplasm and display a different ultra architecture that changes during germination

Spore germination is the transition of dormant spores toward metabolically active and dividing vegetative yeast cells. Spores and vegetative cells differ in terms of morphology and this morphology gradually changes through time. Spores are spherical and highly refractile (Figure 1A), and darken and start growing quickly after the initiation of germination which can be induced by transferring cells to rich media. The hallmark of the completion of germination and the return to vegetative growth is bud emergence, which occurs at about 6 hours after induction of germination (Figure 1A). Cells' transition from high to low refractility correlates with the decrease in optical density at 595 nm (A_{595}) of the pure spore culture (Plante and Landry, 2020b), with the minimal values reached about 3 hours after induction (Figure 1B). One of the adaptive features of spores is their resistance to heat. This feature is lost during germination. The quantification of heat-shock resistance during germination highlights a drastic cellular transition as early as one hour after induction, at which point resistance to thermal stress decreases and reaches levels that compare to that of vegetative cells (Figure 1C). Altogether, these measurements define the time-frame and the major time-points can be used to examine the underlying cellular and molecular changes.

We obtained a more detailed view of the inner cell during germination using transmission electron microscopy (TEM, Figure 1D). Dormant spores are distinguishable by their small size and the thick spore wall absent from vegetative cells. The spore cytoplasm appears darker in TEM in comparison to a vegetative cell, which suggests a denser cytosol (Figure 1D, S1A). Spores have a different cell organization. This is shown by the membranous structures that look highly packed in dormant spores compared to in vegetative cells (Figure 1D). Cells at one and two hours into germination are still indistinguishable from dormant cells. Cell organization changed after about three hours, after heat resistance dropped to levels that compare to that of vegetative cells (Figure 1D). At this time point, there is a rupture of the outer spore wall and the cell starts increasing in size where the spore wall is open. This hatching step is accompanied with a decrease in cytoplasm density and is followed by cell budding. These observations suggest that the spore cytosol organization is timely modulated in the course of germination and return to vegetative growth.

To validate our observations that the density of the cytoplasm decreases during germination, we quantified its viscosity and its dynamic during this process through the examination of macromolecular motion. We expressed the reovirus non-structural protein μNS tagged with GFP as a foreign tracer particle, which has shown to be a suited probe for subcellular environment in yeast (Munder et al., 2016). μNS self-assembles in one or two discrete particles in the yeast cytoplasm that we could detect in both spores and vegetative cells. The tracking of single particles revealed their lower mobility in dormant spores compared to vegetative cells (Figure S2). We calculated a proxy for viscosity from the tracking data of the particles. Because mobility of particles is affected by their size and we observed slight variation in the size of particles during germination (Figure S1A), we corrected for size effect through the calculation of effective viscosity. These measurements confirmed what was seen in the TEM images: dormant spore cytoplasm is the densest among all of these stages. Its median viscosity is 1,250 mPa*s and remains constant in the first two hours of germination, then drops gradually from hatching (3 hour time-point) until the end of germination (Figure 1E). At bud emergence, median viscosity (82 mPa*s) is close to the viscosity measured in vegetative cells (43 mPa*S). These values for vegetative cells are in line with the broad range of viscosity measured in different eukaryotic cells (from 1 to 50 mPa*s (Madshus, 1988; Molines et al., 2022)) and highlights that dormant spores have an exceptionally dense and viscous cytosol. These observations are in the same range as spore viscosity of the fungi *Talaromyces macrosporus*, where spores are found to be characterized by high viscosity (Dijksterhuis et al., 2007).

Stress response in yeast includes cytoplasm acidification that culminates with its rigidification (Munder et al., 2016), including during heat shock (Triandafillou et al., 2020). We therefore hypothesized that the high viscosity of the spore cytoplasm and heat shock resistance would be accompanied by a low pH that would increase during germination. To track this property, we constitutively expressed the pH biosensor superfold-pHluorin (Miesenböck et al., 1998), in both vegetative cells and spores after calibrating pHluorin fluorescence *in vivo*. We estimated pH to be around 5.9 in dormant spores, confirming previous reports (Aon et al., 1997; Barton et al., 1980). Over the course of germination, the cytosol is gradually neutralized (Figure 1F). As soon as one hour after exposure to rich media, median intracellular pH raises to 6.2 and it slowly increases until the end of the process (pH_i = 7.3). At this point, intracellular pH gets close to that measured in vegetatively growing cells (pH_i = 7.4).

Altogether, these experiments show that extreme physicochemical conditions prevail in dormant spores compared to vegetative cells, namely a highly viscous and acidic cytoplasm. These conditions are timely modulated during the germination and return to vegetative growth. These intracellular properties that change during germination can play a critical role in cellular function and organization as they are some of the determinants of protein phase separation (Persson et al., 2020). Protein phase separation was shown to underlie heat shock response in yeast and many other forms of stress responses during cell dormancy (Franzmann and Alberti, 2019). We therefore hypothesized that proteins could have a different solubility in spores and that the modification of physicochemical properties during germination affect their behaviour.

Protein solubility changes during germination

We adopted a physical separation technique similar to the one used in the context of heat shock to measure biochemical changes in protein solubility proteome-wide (Wallace et al., 2015). Protein sedimentation was driven by ultracentrifugation, and protein partitioning between the pellet and supernatant fractions was quantified by liquid-chromatography-coupled tandem mass spectrometry (LC-MS/MS, Figure 1A). We measured the proportion of each protein that partitioned in the pellet fraction using P_{index} as a proxy for desolubilization in three biological replicates and at 5 time-points during germination. In total, we detected 24,559 unique peptides corresponding to 2,614 proteins across the experiment. We restricted our analysis to the 895 proteins with at least two unique peptides that were detected at every time-point to measure P_{index} (Table S2). Values for these 895 proteins range from 0 to 1, which respectively mean that all of the protein is found in the supernatant and all of the protein is found in the pellet. Proteins with low P_{index} are referred to as soluble proteins, while proteins with high P_{index} as less soluble ones. Replicated measurements were strongly correlated (Figure S2A).

We examined the properties of proteins that associate with these changes in solubility. Proteins that change solubility are not more or less abundant than other proteins (Figure S2B). Principal component analysis (PCA) revealed that of all the protein properties considered, propensity for condensate formation (PSAP, (van Mierlo et al., 2021)) and score for prion-like domains prediction (PLAAC, (Lancaster et al., 2014)) are the ones that contribute the most to the separation of proteins in terms of P_{index} (Figure 2C, S2C). Insolubility does not necessarily reflect phase separation as protein solubility is also influenced by many other factors such as misfolding, formation of protein/RNA granules, or other homogeneous or heterogeneous oligomerization. However, because prion-like domains can contribute to protein phase-separation and tune the dynamics of biomolecular condensate (Holehouse et al., 2021), and because propensity for condensate formation positively correlates with P_{index}, high P_{index} estimates at least partially reflect phase-separation of proteins and macromolecular assemblies.

Five typical P_{index} trajectories were identified using hierarchical clustering (Figure 2B). The two largest clusters contain proteins that remain mostly in the supernatant (soluble proteins, n=359) and mostly in the pellet fraction (n=425). Together, they account for 87% of total proteins we considered in our analysis. This means that most of the proteins do not exhibit detectable changes in physicochemical partition during germination using our approach. However, some clusters showed dynamic changes across the time frame examined. First, 15 proteins showed a transient solubilization early in germination. These proteins predominantly partitioned in the pellet in dormant spores, while one hour after exposure to rich media, their P_{index} dropped drastically before rising again at the three-hour time-point and remained insoluble until the end of germination. This group includes for instance the translation initiation factor Cdc33 and the GTP-binding protein Ras2. Another group of 17 proteins gradually desolubilize in the course of germination. They start with high solubility (low P_{index}) in dormant spores, and gradually reach higher P_{index} value at later time-point in the process. This group includes for instance the transcription elongation factor Spt5 and the vacuolar carboxypeptidase Cps1. Finally, 79 proteins with varying single trajectories gradually gained solubility during germination.

Many classes of proteins change solubility during germination, including metabolic enzymes

To understand the functional significance of change in P_{index}, we searched for gene ontology (GO) terms enrichment in three clusters that display dynamic change using the total protein considered for our analysis as a reference set. In the case of the transient solubilization and gradual desolubilization groups, we found significant enrichment for lipid binding and phosphatidylinositol-3-phosphate (PI3P)-binding proteins, respectively (Figure 3A). Since there is no enrichment of integral membrane proteins, there was likely minimal membrane contamination in the cell extracts. Instead, we suspect that the modulation in solubility we detect in these proteins are a reflection of the gain of activity of many cellular pathways. For instance, gradual insolubility of the SNARE chaperone Sec18, involved in vesicle transport from endoplasmic reticulum to golgi, may reflect increasing vesicle transport required to sustain growth. The larger group of proteins with increasing solubility is enriched for proteins with catalytic activity: precisely, oxidoreduction and protein phosphatase activity (Figure 3A), including for instance the ceramide-activated protein phosphatase Sit4 which functions in the G1/S transition in cell-cycle (Barbosa et al., 2016). This may reflect the reentry of the dormant spores in the cell cycle. Among this group, we also identified the stress related proteins Ola1 and Yef3, which are known to aggregate in response to heat stress (Wallace et al., 2015). The behaviour of these proteins suggest that dormancy in spores shares features with stress response and that germination would correspond to stress relief. Within the group of proteins with increasing solubility, we identified enzymes involved in carbohydrate, lipid and nitrogen metabolisms (Figure 3B). Since nutrient starvation is the key signal that triggers sporulation, the comportment of these metabolic enzymes that solubilize in the course of germination caught our interest. We investigated two of them: the CTP synthase Ura7 and the acetyl-CoA carboxylase Acc1, which are enzymes known to form high molecular weight assemblies in response to nutrient starvation (Narayanaswamy et al., 2009; Petrovska et al., 2014). To validate the solubility changes revealed by P_{index} trajectories, we generated cells expressing either Ura7 or Acc1 tagged - at their genomic locus - with GFP. Both Ura7 and Acc1 formed cytoplasmic foci in dormant spores (Figure 3C). Upon germination, Ura7-GFP and Acc1-GFP fluorescence signals changed until they became mostly diffuse in dividing cells. This behavior confirms the dissolution of the protein assemblies observed in the P_{index} trajectories. In addition, we noted the opposite behavior of the glucokinase Glk1. Glk1's P_{index} trajectory suggests it gains insolubility during germination. Correspondingly, we found Glk1-GFP to be diffuse in dormant spores, then appears as dense assemblies in cells as soon as one hour after exposure to rich media and until the end of germination. Glk1 was found to polymerize and form filament during the transition from low to high sugar conditions (Stoddard et al., 2020). Its behavior in germinating cells again suggest that spores remain dormant in a starved form and that breaking of dormancy implies changes of enzyme biophysics in response to nutrient repletion.

The reverse order of events between spore germination and heat stress and nutrient stress responses for some key proteins suggest a model in which spores are dormant in a stress response state and germination corresponds to stress relief and return to normal vegetative growth (Figure 3D). Spores therefore most likely borrow strategies from vegetative cells for stress resistance.

The heat shock protein Hsp42 shows dynamic solubilization and phosphorylation during germination

To further explore the regulatory mechanisms driving cellular reorganization during germination, we searched in our proteomic data for phosphorylation on tyrosines, serines or threonines. We identified 36 phosphoproteins with a unique phosphopeptide in at least one time point during germination (Figure 4A). Given that we did not perform any enrichment for phosphorylation prior to mass spectrometry, the detection of a limited number of phosphorylation was expected. These include for instance the topoisomerase Top1 and the transcription elongation factor Spt5. Out of the 36 phosphoproteins, one is the small oligomeric heat shock protein (sHSP) Hsp42. Since stress response in vegetative cells involves sHSP and they were recently identified as key players in the resolution of molecular assemblies that accompany heat shock (Yoo et al., 2022), we focused on this protein as a potential regulator of protein solubilization in germination.

Hsp42 is part of the protein clusters with changing solubility during germination. Furthermore, the solubility of Hsp42 is correlated with its phosphorylation during this time-period. Solubility transiently increases while abundance of its phosphorylation transiently increases (Figure 4B). Hsp42 was shown to reversibly assemble in heterogeneous granules in a heat-induced manner, or in quiescent cells in stationary phase (Liu et al., 2012), and to function in tuning granules assembly and disassembly (Grousl et al., 2018). Remarkably, Hsp42-dependent spatial protein organization is crucial for cellular fitness, and lack in foci formation results in a significant delay when recovering from stationary phase (Liu et al., 2012). We hypothesized that the dynamic in Hsp42 localization we observed reflects its function during germination.

To confirm the dynamic assembly and disassembly of Hsp42 during germination, we generated cells expressing Hsp42 fused to GFP. Hsp42 accumulates in cytoplasmic foci in dormant spores, which corroborates its solubility in the proteomics experiments. One hour after the induction of germination, Hsp42 is diffused, which shows the dissolution of the foci (Figure 4D). Diffused localization of Hsp42 is only transient since foci were visible at later time-point during vegetative growth. Microscopic observations therefore validate the P_{index} profile of Hsp42, suggesting a transient modification of the protein taking place early in germination.

The search for phosphorylation sites from the proteomics data revealed a dynamic phosphorylation site located in the N-terminal region (NTR) of Hsp42 (S223). Disorder profile of Hsp42 highlights three structurally distinct domains; a central structured domain that is predicted to a alpha-crystallin domain (ACD) common to sHSP, and a long N-terminal region (NTR) and a short C-terminal regions that are both predicted to be highly disordered (Haslbeck et al., 2019). Structure prediction of Hsp42 (Uniprot Q12329) (Jumper et al., 2021) corroborates this architecture; it predicts with high confidence a beta-strand sandwich typical of ACD but predicts large unstructured parts in the N and C-terminal regions (Figure 4E). NTRs are shown to be involved in the regulation and dynamics of chaperone activity of sHSP (Haslbeck et al., 1999, 2019). These proteins are stored in an inactive form as high-order oligomers, and their activation involves phosphorylation, especially in the NTR, that drives disassembly of sHSP into smaller complexes. For instance, several phosphorylation sites on Hsp26 were found to activate chaperon activity by weakening interactions within the oligomers (Mühlhofer et al., 2021). The phosphorylation of S223 on Hsp42 has been previously detected by mass spectrometry. The abundance of this phosphorylation was found to increase in cells following exposure to heat (Kanshin et al., 2015). Hence, we hypothesized that the phosphorylation on S223 of Hsp42 is involved in this sHSP's role during the major cytoplasmic changes that take place during germination.

We first confirmed that Hsp42 plays an important role in thermal stress protection, and if S223 phosphorylation may be regulating this function in vegetative cells (Grousl et al., 2018; Haslbeck et al., 2004). After being subjected to a heat shock, cells lacking Hsp42 (*hsp42*Δ::kanMX4) fail to grow as compared to WT cells, confirming thermal sensitivity (Figure 5A). A phosphomimetic mutant of Hsp42 (S223E) appears to be equally active as the WT chaperon, because expression of either protein tagged with GFP totally restores cellular heat shock resistance (Figure 5A). On the other hand, mutation of the site to a non-phosphorylatable residue (S223A) seems to impede chaperon activation or activity as revealed from the mutant phenotype. Cells expressing the Hsp42 S223A mutant show thermal stress sensitivity (Figure 5A) and this mutant fails to form large cytoplasmic foci as does the protective Hsp42 (Figure 5B). These results suggest that this phosphorylation site could be important during germination. We therefore tested if Hsp42 activity was crucial during germination. Optical density decrease of *hsp42*Δ spores culture exposed to germination conditions is delayed compared to WT spores, suggesting a delay in germination (Figure 5C). In addition, microrheology revealed that *hsp42*Δ spores decrease their viscosity in a delayed fashion compared to WT spores (Figure 5D).

We tested how this delay in biophysical remodeling in *hsp42*Δ spores affected protein organization. In WT spores, Acc1-mCherry is diffusely localized four hours after exposure to rich media. In contrast, in *hsp42*Δ spores, Acc1-mCherry remains condensed as foci (Figure 5E). These results show a role for Hsp42 in disassembly of Acc1 foci. Expression of either WT or a phosphomimetic mutant (S223E) of Hsp42 totally rescues the germination progression in *hsp42*Δ spores (Figure 5C) and restores the disassembly of Acc1 foci (Figure 5F). On the other hand, spores expressing the non-phosphorylatable S223A mutant experienced a delayed germination, and in these cells, Acc1 foci failed to disassemble (Figure 5F). In addition to the role of Hsp42 in facilitating protein dissolution under stress conditions (Grousl et al., 2018) we unveil its function key actor for the solubilization of low solubility proteins such as the acetyl-CoA carboxylase Acc1. Altogether, these findings indicate that the presence and the phosphorylation of Hsp42 on S223 play a critical role in the progression of germination and in the remodeling of the cytoplasm biophysics

Conclusion

Some dormant cells have exceptional resistance to stress. What are the biophysical conditions that underlie these properties and how cells resume growth after dormancy are important questions across fields of biology. In this work, we used yeast spores to examine the biophysical properties of a dormant cytosol and its transition between dormancy and its return to vegetative growth. The spore cytosol is acidic and highly viscous, as has been observed in the context of various stresses, for instance in yeast cells during energy depletion (Munder et al., 2016), bacteria during metabolic arrest (Parry et al., 2014), dry plant seed (Buitink and Leprince, 2008), and tardigrades during desiccation (Boothby et al., 2017). The properties observed in yeast spores may therefore represent a conserved adaptive strategy for many cell types and species.

Because of the commonalities with the properties of yeast cells responding to stress, spores' cytosolic properties reflect that spores are in metabolic repression and stress response state. During germination, cells come back to an unstressed state where spore cytosol is neutralized and its viscosity decreased. We also found massive altered protein organization in dormant spores that changes along with the cytosol pH and viscosity during germination. Germination therefore shares many features with stress relief, for instance after heat shock in vegetative cells. One important question these observations trigger is what are the early molecular events that allow the cytosol and the solubility of many proteins to progressively change during germination. We identified Hsp42 as a key actor for the modulation of spore cytosol organization. The role of Hsp42 in dissolution of enzyme assembly during germination extends the role of chaperones in the disassembly of heat-induced protein condensate recently shown (Yoo et al., 2022). The role of heat shock proteins in response to stress in vegetative cells may thus also be critical to the breaking of dormancy of spores, which have intrinsically high stress resistance. The dissolution of insoluble metabolic enzymes during this transition likely reflects the activation of spore metabolism as it modifies its physiology to respond to nutrient, and is an adaptation to nutrient repletion (Petrovska et al., 2014). We identified the phosphorylation of Hsp42 at S223 to be critical for its regulating function in protein organization. This post-translational modification has been reported multiple times in phosphoproteomic analysis (Martínez-Montañés et al., 2020; Swaney et al., 2013), notably in the context of heat shock where cells in unstressed conditions show low levels of Hsp42 phosphorylation while under stress conditions they quickly accumulate phosphorylated Hsp42 (Kanshin et al., 2015). Regarding these observations, the Hsp42 profile we report shows that early in germination spores exhibit stress response, and that while gemination progresses, stress response is relieved. The dynamic modulation in phosphorylation of Hsp42 we report implies that prior signaling steps including kinase activity upstream are required for the adaptation of spore cytosol organization to nutrient repletion. Therefore, Hsp42 presumably functions in adapting spore cytosol to nutrient repletion in a similar manner as Floe1 integrates the signal of adequate hydration in *A. thaliana* seed to control germination (Dorone et al., 2021).

Altogether, our results expand our knowledge of the molecular factor taking part in dissolution of protein assemblies, and sheds light into the regulation of protein condensate through signaling. Signaling and kinase activity has been previously linked with protein organization in the context of cellular stress (Wippich et al., 2013). Stress-induced phosphorylation of human Hsp27 was shown to cause its phase separation with FUS, a process that was found to prevent FUS amyloid fibril formation (Liu et al., 2020). Phosphorylation of Hsp42 could imply the mitogen-activated protein (MAP) kinase signaling pathway, which has been reported to be involved in human Hsp27 phosphorylation (Liu et al., 2020). Some kinases in yeast, notably cyclin-dependent kinases Cdc28 and Pho85 or MAP kinases Hog1 and Fus3, have specificities that correspond to the phosphorylation site motif of Hsp42 S223 (Mok et al., 2010). In addition, a target of the MAP kinase Hog1, the transcription elongation factor Spt5 (Silva et al., 2017), does show a similar profile of phosphorylation during germination (YML010W, Figure 4A). Connecting upstream kinases to the activity of Hsp42 will eventually allow to connect nutrient sensing of activating spores and the biophysics of spore cytoplasm.

Cell dormancy is widespread across the three of life and is a survival strategy for many species facing harsh conditions and pathogens (Ortiz et al., 2019) and cancer cells facing drug treatment (Oren, 2022). By discovering what are the early events that regulate the breaking of dormancy, our work will help better understand the molecular basis of adaptation to extreme conditions and potentially help find ways to develop drugs or conditions that can potentiate existing drugs to overcome their exceptional resistance mechanisms.

Acknowledgments

We thank Daniel Evans-Yamamoto, David Bradley and Alexandre K. Dubé for their comments on the manuscript, and Alexandre K. Dubé and Isabelle Gagnon-Arsenault for their support in the laboratory. We are grateful to Pr Martin Bisaillon, from Université de Sherbrooke (Canada) for providing us the µNS coding sequence. This work was supported by NSERC Discovery Grants to CRL and LJF, a Canadian Institutes of Health Research (CIHR) Foundation grant (387697) to CRL, and platform funding from Genome Canada (264PRO) to LJF. CRL holds the Canada Research Chair in Cellular Synthetic and Systems Biology.

Authors contributions

Conceptualization: CRL and SP

Methodology and Experiments: SP, KMM, PL, LJF
Validation: SP
Formal analysis: SP, KMM
Writing – original draft preparation: SP, CRL
Writing – review and editing: all authors
Visualization: SP
Supervision: CRL and LJF
Project administration: CRL
Funding acquisition: CRL and LJF

STAR Methods

Key resource table

REAGENT or RESOURCE	SOURCE	IDENTIFIER
Chemicals, peptides, and recombinant proteins		
cOmplete, EDTA-free Protease Inhibitor Cocktail	MiliporeSigma	cat#11836153001
Percoll	MiliporeSigma	cat#P1644
Nigericin	MiliporeSigma	cat#481990
2-Deoxyglucose	Bioshop	cat#DXG498
Concanavalin A	MiliporeSigma	cat#C2010
Critical commercial assays		
BCA Protein Assay Kit	Novagen	Cat#71285
Deposited data		
Raw and analyzed mass spectrometry data	Data are available via ProteomeXchange	PXD035403
Experimental models: *Saccharomyces cerevisiæ* strains		

LL13_054 wild diploid strain MATa/***α***	(Leducq et al., 2016)	LL13_054
ura3::P*SOD1*-μNS-GFP hphNT1 (background: LL13_054)	This Paper	SPY020
ura3::P*SOD1*-sfpHluorin hphNT1 (background: LL13_054)	This Paper	SPY031
ACC1-GFP::hphNT1 (background: LL13_054)	This Paper	SPY037
URA7-GFP::hphNT1 (background: LL13_054)	This Paper	SPY039
HSP42-GFP::hphNT1 background: LL13_054)	This Paper	SPY040
GLK1-GFP::hphNT1 (background: LL13_054)	This Paper	SPY044
hsp42Δ::KanMX4 (background: LL13_054)	This Paper	SPY056
hsp42Δ::HSP42-GFP-hphNT1 (background: LL13_054)	This Paper	SPY078

hsp42Δ::HSP42(S223A)-GFP-hphNT1 (background: LL13_054)	This Paper	SPY080
hsp42Δ::HSP42(S223D)-GFP-hphNT1 (background: LL13_054)	This Paper	SPY081
ACC1-mCherry::natNT2 (background: LL13_054)	This Paper	SPY089
hsp42Δ::KanMX4 ACC1-mCherry::natNT2 (background: LL13_054)	This Paper	SPY093
hsp42Δ::HSP42-GFP-hphNT1 ACC1-mCherry::natNT2 (background: LL13_054)	This Paper	SPY101
hsp42Δ::HSP42(S223A)-GFP-hphNT1 ACC1-mCherry::natNT2 (background: LL13_054)	This Paper	SPY102
hsp42Δ::HSP42(S223D)-GFP-hphNT1 ACC1-mCherry::natNT2 (background: LL13_054)	This Paper	SPY103
Oligonucleotides		

Primers used in this study are listed in table S1	This study	N/A
Recombinant DNA		
Plasmid: pYM25	PCR tool box	Janke et al., Yeast, 2004
plasmid: pYM25-PSOD1-µNS-yeGFP	This study	N/A
plasmid: pYM25-PSOD1-sfpHluorin	This study	N/A
plasmid: pUG6	Euroscarf	P30114
plasmid: pNATCRE	(Steensma and Ter Linde, 2001)	pNATCRE
plasmid: pBS35 (mCherry) + natNT2	Addgene	Cat#83797
plasmid: pYM25-HSP42-GFP	This study	N/A
plasmid: pYM25-HSP42(S223A)-GFP	This study	N/A
plasmid: pYM25-HSP42(S223D)-GFP	This study	N/A
Software and algorithms		
Rstudio	Rstudio	RRID: SCR_000432 (https://www.rstudio.com/)
Python (v 3.7.4)	Python	https://www.python.org/
GrowthCurver (v 0.3.1)	(Sprouffske and Wagner, 2016)	https://github.com/sprouffske/growthcurver
TrackPy (v 0.5.0)	(Crocker and Grier, 1996)	http://soft-matter.github.io/trackpy/v0.5.0/
Matplotlib (v 3.5.1)	(Hunter, 2007)	https://matplotlib.org/

Seaborn	(Waskom, 2021)	https://seaborn.pydata.org/index.html
Prion-Like Amino Acid Composition (PLAAC)	(Lancaster et al., 2014)	http://plaac.wi.mit.edu
scipy.cluster.hierarchy (v1.8.1)	Scipy	https://docs.scipy.org/doc/scipy/reference/cluster.hierarchy.html
Metapredict (v2.0)	(Emenecker et al., 2021)	https://github.com/idptools/metapredict
Phase Separation Analysis and Prediction (PSAP)	(van Mierlo et al., 2021)	https://github.com/Guido497/phase-separation).
Scikit-learn (sklearn) v1.1.1	(Pedregosa et al., 2011)	https://scikit-learn.org/

Method details

Yeast strains construction and culture conditions

The yeast strains used in this study are listed in the Key resources table. Background for every construction is the wild diploid *Saccharomyces cerevisiae* LL13_054 (Leducq et al., 2016). This strain was chosen for its propency to sporulate at high efficiency. For C-terminal labeling of Acc1, Ura7, Glk1 and Hsp42 with GFP at their native genomic locus (Figure 3C, 4D), GFP and Hyg resistance marker (hphNT2) were amplified from pYM25 with flanking DNA for genomic integration. For deletion of *HSP42* (Figure 5, *hsp42*∆) the cassette loxP-pAgTEF1-kanMX-tAgTEF1-loxP from pUG6 was amplified with the flanking DNA for replacement of the HSP42 coding sequence, leaving its promoter and terminator intact. The deletion cassette was removed by expressing the recombinase Cre on the plasmid pNatCRE. Site-directed mutagenesis on Hsp42 (S223A or S223E) was conducted by primer extension. For restoration of Hsp42 expression in hsp42∆ cells (Figure 5A, B, C, F), WT or mutant HSP42 coding sequences (excluding stop codon) were cloned in pYM25 upstream and in frame with GFP using Gibson assembly. HSP42(WT or mutant)-GFP-hphNT2 was amplified with flanking DNA for integration designed to introduce HSP42-GFP downstream of HSP42 promoter at its native genomic locus in the hsp42∆ strain. For C-terminal labelling of Acc1 with mCherry at its native genomic locus (Figure 5E, F) mCherry-natNT2 was amplified from pBS35 + natNT2 plasmid with adequate flanking sequence for integration. Primer used for strains construction are listed in table S1. At each step, diploid cells were sporulated, and haploid spores were dissected on selection media and further sequencing and microscopic analysis confirmed integration. Culture from confirmed spores gave rise to homozygous diploid cells as these are homothallic spores. Competent cells were prepared and transformations performed using standard protocols (Amberg et al., 2005). Yeast were grown in YPD medium containing 1% yeast extract (Bioshop), 2% peptone (Bioshop), and 2% glucose (Bioshop) with the appropriate antibiotic selection.

Sporulation and germination

Sporulation was conducted on sporulation medium plates containing 1% potassium acetate, 0.1% yeast extract, 0.01% glucose, and 2% agar and spores were further purified on Percoll gradient (Sigma) as previously described (Plante and Landry, 2020b). Germination was induced by transferring spores to YPD. To monitor germination, fresh spores were diluted in YPD at an OD_{600} = 1 and optical density was measured periodically in an Infinite M Nano plate reader (Tecan) set at 30˚C.

Heat shock resistance assay

Resistance measurements in spores during germination (Figure 1B) were conducted as described previously (Plante and Landry, 2020b). Briefly, freshly purified wild spores were induced in germination in YPD medium, and at the indicated time following induction cells were sampled. Half of the cells were diluted in YPD medium, and the other half was treated at 55˚C for 10 minutes in a thermocycler (Eppendorf Mastercycler ProS) before being transferred to YPD. Growth curves of both treated and untreated cells were recorded in an Infinite M Nano plate reader (Tecan) set at 30˚C without shaking. Area under the curve (AUC) was determined using the Growthcurver package in R (Sprouffske and Wagner, 2016). Heat resistance value was defined as the ratio of AUC of treated growth curve to AUC of untreated growth curve both obtained over the time required for untreated spore ODs to reach stationary phase. For resistance measurement of vegetative cells (Figure 5A), cells were grown overnight in YPD and diluted in YPD at OD_{600} of 0.1 and grown at 30˚C until they reached an OD_{600} of 0.4 - 0.5. Equal amounts of cell were diluted in fresh YPD medium, or incubated at 50˚C for 10 minutes in a thermocycler prior to dilution. Growth curves of treated and control cells were recorded in a plate reader set at 30˚C.

Phase contrast and fluorescence cell imaging

All microscopic imaging experiments were performed using eight-well glass-bottom chamber slides (Sarstedt) coated with 0.05 mg/ml concanavalin A (Millipore Sigma). For phase contrast observation of germination (Figure 1C), freshly prepared spores were induced in germination by transferring them in a chamber filled with YPD medium. Cell imaging was performed on an Apotome Observer Z1 microscope (Zeiss) equipped with LD PlnN 40x/0.6 objective (Zeiss) at the indicated time after induction in a single field. For fluorescence observation during germination, freshly prepared spores were diluted in YPD medium and incubated at 30℃. At the indicated time after exposure to germination conditions, spores were washed in water, and transferred in a chamber filled with SC medium containing 0.174% Yeast nitrogen base (BioShop), 2% glucose and 0.5% ammonium sulfate (BioShop). For fluorescence observation on vegetative cells (Figure 5B), cells were grown in YPD at 30℃ until they reached an OD_{600} of 0.4 - 0.5. Cells were left untreated (Control) or subjected to a heat shock at 50°C for 10 minutes in a thermocycler. They were then washed in water and transferred in a chamber filled with SD medium. Fluorescence imaging was performed on an Apotome microscope equipped with a Plan-Apochromate 100x/1.4 oil objective (Zeiss). Image acquisition was performed using an AxioCam MRm camera (Zeiss). Images were analysed using the ImageJ software (Schneider et al., 2012).

Transmission Electron microscopy

Freshly prepared spores were induced in germination in YDP at 30˚C. At the indicated time after the induction of germination, cells were harvested, washed in water and suspended in fixative solution, containing 2.5% glutaraldehyde, 1.5% paraformaldehyde, 0.5mM $CaCl_2$ in 0.1M caco buffer pH 7.2. Vegetatively growing cells in YPD (OD600 = 0.5-0.6) were harvested, washed in water and suspended in fixative solution. Cells were fixed for 24 hours at room temperature. Following steps were conducted by the microscopy platform of IBIS (Université Laval, Québec, Canada). Cells were dehydrated with ethanol solution (30-100%), then embedded in epoxy resin (Epon). 150 nm–thick sections of resin-embedded cells were prepared using an ultramicrotome (Ultracut UCT; Leica), and stained with 1% (wt/vol) uranyl acetate in 70% (wt/vol) methanol for 5 min and 0.4% lead citrate for 3 min. Samples were imaged on a JEM 1230 Transmission Electron Microscope (JOEL). Images were analysed and processed using ImageJ software.

Molecular probes

The complete sequence of mammalian orthoreovirus 3 strain T3 non structural protein µNS (GeneBank MK246417.1) was kindly shared by Pr. Martin Bisaillon from Université de Sherbrooke. We cloned by gibson assembly the whole coding sequence, minus stop codon, into pYM25 (Janke et al., 2004) to generate a fusion with yeGFP at its C-terminus. The promoter of *SOD1* (nucleotides -851 to -1 relative to ATG) was cloned by Gibson assembly upstream the µNS CDS in pYM25. Expression of SOD1 was shown in spores and during germination (Plante et al., 2017), and expression of the

molecular probe with this promoter happened at a high level in spores and during germination which suited our experiments with this cell type. *SOD1* promoter - μNS - GFP in addition to HPH markers on pYM25 were amplified as a whole with the appropriate flanking sequences for genomic integration at the *URA3* locus. From all tested loci for integration (*MET15*, *LEU2*, *HIS3*), *URA3* allows high and uniform expression of the probes across the population, while having the least effect on sporulation and germination efficiency.
Plasmid p426MET25 containing sfpHluorin gene was purchased from Addgene (ID 115697). We swapped the yeGFP gene in pYM25 plasmid for sfpHluorin, and cloned the *SOD1* promoter upstream the sfpHluorin CDS by Gibson assembly. The *SOD1* promoter - sfpHluorin in addition to HPH marker on pYM25 were amplified as a whole with the appropriate flanking sequences for genomic integration at the *URA3* locus. Yeast with either genomic integration were selected for hygromycin resistance.

Particle tracking and microrheology
Cells expressing *μNS*-GFP were transferred to a 8-well glass-bottom chamber slides (Sarstedt) coated with concanavalin A 0.05 mg/mL (Millipore Sigma) and filled with 500μl of complete SC medium. Image acquisition was performed using a Perkin Elmer UltraVIEW confocal spinning disk unit attached to a Nikon Eclipse TE2000-U inverted microscope equipped with a Plan Apochromat DIC H 100×/1.4 oil objective (Nikon), and a Hamamatsu Orca Flash 4.0 LT + camera. Imaging was done at 30 °C in an environmental chamber. The software NIS-Elements (Nikon) was used for image capture. For each field, one brightfield and a series of fluorescence (GFP) images were taken. Cells were excited with a 488 nm laser and emission was filtered with a 530/630 nm filter. GFP time lapse images were acquired continuously at a rate of two frames/sec for one min. Images were processed using image J. Particle tracking was performed using the python package Trackpy ((Crocker and Grier, 1996), http://soft-matter.github.io/trackpy/v0.5.0/). Particles were identified in microscopic images using the “locate” function. Minimal mass threshold was set at 200 to exclude spurious fluorescence signals. Trajectories were assembled from the multiple frames using the “link” function. The “imsd” function was used to compute mean squared displacement of individual particles. Microns per pixel was set as 10/75 and frames per second = 2. From the Stokes-Einstein relation (Figure 1E) we computed the effective viscosity (η) as:

$$\eta = \frac{\kappa_B T}{6\pi D r}$$

where κ_B is the Boltzmann constant, T is the temperature (303 K), D is the displacement constant obtained from MSD of a given particle and r is the radius that particle.

Intracellular pH measurements

Exponentially growing wild type cells expressing sfpHluorin (OD = 0.3-0.4) in YPD medium were used for calibration curve determination as previously described (Triandafillou and Drummond, 2020). Cells were washed twice in water and suspended in calibration buffer containing 50 mM NaCl, 50 mM KCl, 50 mM MES, 50 mM HEPES, 100 mM ammonium acetate, 10 mM 2- deoxyglucose and 10 µM nigericin; pH was adjusted with HCl or KOH from 5.0 to 9.0. After 30 minutes incubation at room temperature, fluorescence (533 nm) of sfpHluorin following excitation at 405 and 488 nm was acquired using a Guava EasyCyte HT cytometer (EMD Millipore). The calibration curve was generated by taking the median ratio of fluorescence after excitation at 405 nm to excitation at 488 nm (405/488 ratio) at various pH. Ratios were corrected for background by subtracting the autofluorescence of unlabeled cells (WT). Points were fitted to a sigmoid (Figure S1D). pH measurement was performed on vegetatively growthing cells (OD=0.3-0.4) expressing sfpHluorin in YPD and freshly prepared spores expressing sfpHluorin at the indicated time-points after exposure to rich medium. Cells were washed twice in water then suspended in a measurement buffer containing 50 mM NaCl, 50 mM KCl, 50 mM MES, 50 mM HEPES, 100 mM ammonium acetate. After 30 minutes of incubation at room temperature, the median 405/488 ratio was measured by cytometry. pH values were obtained from the sigmoid function of the calibration curve.

Protein extraction and sedimentation.

Freshly purified wild spores at the indicated time following germination induction in YPD medium, and vegetatively growing cells in YPD (OD = 0.5-0.6) were harvested. Cell were resuspended in 4 ml Protein buffer containing 120 mM KCl, 2 mM EDTA, 20 mM HEPES-KOH, pH 7.4, 1:500 Protease inhibitor (MiliporeSigma), 0.5 mM DTT and 1mM PMSF, and snap frozen as 20 µL beads, then placed in a 10 ml milling pod (Retsch) cooled in liquid nitrogen along with a 10 mm milling bead. 20 milling cycles of 2 minutes each each were performed on a Mixer Mill MM 400 (Retsch) at 30 Hz, with cooling in liquid nitrogen between each cycle. Cell extracts were thawed on ice, and clarified by centrifugation at 16,000 g for 10 minutes. Supernatant was retrieved and protein concentration was measured by BCA protein assay (Novagen, (Smith et al., 1985). Protein concentrations were adjusted in all the samples to 800 µg/ml. Equal volume (2 ml *i.e* 1600 µg) of cell extracts were loaded in ultracentrifuge tubes (Beckman). Samples were ultracentrifuged at 100,000 g for 30 minutes at 4˚C in a Optima XPN-100 ultracentrifuge (Beckman). Supernatants were kept aside as “Supernatant” fraction. Pellets were washed twice with protein buffer, then resuspended in protein buffer + 1% SDS which correspond to “Pellet” fraction. 1% of total supernatant (i.e. 20 µl) and pellet fraction (i.e. 10 µl) for each cell extract was loaded on a 10% SDS-polyacrylamide gel in a loading buffer containing 0.06M Tris pH 6.8, 0.07M SDS, 10% glycerol, 5% 2-mercaptoethanol and 0.01% bromophenol blue. Migration was conducted at 90 V until dye front reached 1 cm into the gel. Proteins were stained with Coomassie G-250 dye, and lanes were cut out of the gel and stored in 1.5 ml microtubes before they are further processed.

Mass spectrometry

In gel protein digestion was performed as previously described (Shevchenko et al., 1996). Gel lanes of each sample were cut into smaller pieces, destained with 40% ethanol in 30 mM ammonium bicarbonate then reduced with 10 mM DTT at 37°C for 30 min then alkylated with 55 mM iodoacetamide at 37°C for 30 min. The gel pieces were digested at 37°C initially with 0.5 µg of trypsin (Promega) per sample for 6 hours then additionally with 0.3 µg of trypsin overnight. The resulting peptides were extracted from gel pieces using sequential shaking in 40% acetonitrile then 100% acetonitrile, vacuum centrifuged (Vacufuge, Eppendorf) to evaporate the organic solvents and cleaned through C18 STop-And-Go-Extraction tips (StageTips, PMID 12498253), eluted in 40% acetonitrile, 0.1% formic acid, and vacuum centrifuged until complete dryness.
LC-MSMS analysis (Kerr et al., 2020). The concentration of the final reconstituted sample was measured at A_{205} using a NanoDrop One (Thermo Fisher) to inject 250 ng into Bruker Impact II Qtof coupled to easy nLC 1200 (Kerr et al., 2020). The injection was randomized to minimize loading order bias. A single analytical column set up using IonOpticks' Aurora UHPLC column (1.6 µm C18 and 25 cm long) was used to create 90 minutes of separation from 5% to 35% buffer B for each sample.

Data search.

Resulting data were searched on MaxQuant version 1.6.17.0 (Cox et al., 2009) against sequences from verified and uncharacterized ORFs from the R64-3-1 release of the S288C genome proteome database (yeastgenome.org) and common contaminant sequences provided by the software (246 sequences) adding the following variable modifications: oxidation on methionines, acetylation on protein N-termini, acetylation on lysines, methylations on arginine, and phosphorylation on serines, threonines, and tyrosines. Fixed carbamidomethylation was set on cysteines. Default match between runs was enabled and default peptide and fragment mass tolerances (10 and 40 ppm) were set. Data were filtered to have 1% false discovery rates at peptide and protein levels. The mass spectrometry proteomics data have been deposited to the ProteomeXchange Consortium via the PRIDE (Perez-Riverol et al., 2022) partner repository with the dataset identifier PXD035403.

Proteomic analysis

For the analysis of protein solubility (Pindex measurements) we considered the intensity-based absolute quantification (iBAQ, (Schwanhäusser et al., 2011)) of proteins with sequence coverage of ≥10% with at least 2 peptides. 895 proteins, for which total abundance (Supernatant + pellet) was > 0 in each replicate at every time-points of germination, were included in the analysis. Pindex of a given protein was measured as the ratio of its abundance in the pellet to its total abundance (Supernatant + Pellet). Since Pindex values across the triplicates were highly correlated (Figure S2A), we considered the mean Pindex of each triplicate. Pindex values of the 895 proteins considered at each time-point in germination are listed in Table S2. Clustering of Pindex trajectories was performed in python using the Hierarchical clustering method in the Scipy package (scipy.cluster.hierarchy). Hierarchical linkage was conducted with the linkage function using the "complete" method. The clusters were then defined using the fcluster function using the "distance" criterion for discrimination.

Protein properties

Molecular weight and isoelectric point of the 895 considered proteins were retrieved on web-based YeastMine application (https://yeastmine.yeastgenome.org/). Total iBAQ (Supernatant + Pellet) for each of the 895 proteins in the analysis was average amongst the five time-points to obtain the mean abundance. To measure, in the considered proteins, the amino acid composition predicted to form prion-like domain, we used the Prion-like amino acid composition (PLAAC) web-based application (http://plaac.wi.mit.edu/details, (Lancaster et al., 2014)). From this application, we considered the normalized score (NLLR) of each protein for our analysis. To predict the propensity of each of the proteins to condensate, we used the python application PSAP ((van Mierlo et al., 2021), https://github.com/Guido497/phase-separation). This classifier scores each residue, and we used the median score of each protein for further analysis. To predict the consensus disorder of each protein, we used the python application Metapredict ((Emenecker et al., 2021), https://github.com/idptools/metapredict) which is a neural network trained for single residue scoring. For further analysis, we used the median metapredict score for each protein. Principal component analysis (PCA) was performed using the Scikit-learn package in python. Protein properties data were first scaled using the StandardScaler function, then PCA was performed with PCA function.

References

Amberg, D.C., Burke, D., and Strathern, J.N. (2005). Methods in Yeast Genetics: A Cold Spring Harbor Laboratory Course Manual (CSHL Press).

Aon, J.C., Aon, M.A., Spencer, J.F., and Cortassa, S. (1997). Modulation of sporulation and metabolic fluxes in Saccharomyces cerevisiae by 2 deoxy glucose. Antonie Van Leeuwenhoek *72*, 283–290. .

Barbosa, A.D., Pereira, C., Osório, H., Moradas-Ferreira, P., and Costa, V. (2016). The ceramide-activated protein phosphatase Sit4p controls lifespan, mitochondrial function and cell cycle progression by regulating hexokinase 2 phosphorylation. Cell Cycle *15*, 1620–1630. .

Barton, J.K., den Hollander, J.A., Lee, T.M., MacLaughlin, A., and Shulman, R.G. (1980). Measurement of the internal pH of yeast spores by 31P nuclear magnetic resonance. Proc. Natl. Acad. Sci. U. S. A. *77*, 2470–2473. .

Boothby, T.C., Tapia, H., Brozena, A.H., Piszkiewicz, S., Smith, A.E., Giovannini, I., Rebecchi, L., Pielak, G.J., Koshland, D., and Goldstein, B. (2017). Tardigrades Use Intrinsically Disordered Proteins to Survive Desiccation. Mol. Cell *65*, 975–984.e5. .

Buitink, J., and Leprince, O. (2008). Intracellular glasses and seed survival in the dry state. C. R. Biol. *331*, 788–795. .

Coluccio, A.E., Rodriguez, R.K., Kernan, M.J., and Neiman, A.M. (2008). The yeast spore wall enables spores to survive passage through the digestive tract of Drosophila. PLoS One *3*, e2873. .

Cox, J., Matic, I., Hilger, M., Nagaraj, N., Selbach, M., Olsen, J.V., and Mann, M. (2009). A practical guide to the MaxQuant computational platform for SILAC-based quantitative proteomics. Nat. Protoc. *4*, 698–705. .

Crocker, J.C., and Grier, D.G. (1996). Methods of Digital Video Microscopy for Colloidal Studies. J. Colloid Interface Sci. *179*, 298–310. .

Dijksterhuis, J., Nijsse, J., Hoekstra, F.A., and Golovina, E.A. (2007). High viscosity and anisotropy characterize the cytoplasm of fungal dormant stress-resistant spores. Eukaryot. Cell *6*, 157–170. .

Dorone, Y., Boeynaems, S., Flores, E., Jin, B., Hateley, S., Bossi, F., Lazarus, E., Pennington, J.G., Michiels, E., De Decker, M., et al. (2021). A prion-like protein regulator of seed germination undergoes hydration-dependent phase separation. Cell *184*, 4284–4298.e27. .

Emenecker, R.J., Griffith, D., and Holehouse, A.S. (2021). Metapredict: a fast, accurate, and easy-to-use predictor of consensus disorder and structure. Biophys. J. *120*, 4312–4319. .

Franzmann, T.M., and Alberti, S. (2019). Protein Phase Separation as a Stress Survival Strategy. Cold Spring Harb. Perspect. Biol. *11*. https://doi.org/10.1101/cshperspect.a034058.

García-Roger, E.M., Lubzens, E., Fontaneto, D., and Serra, M. (2019). Facing Adversity:

Dormant Embryos in Rotifers. Biol. Bull. *237*, 119–144. .

Gremer, J.R., and Sala, A. (2013). It is risky out there: the costs of emergence and the benefits of prolonged dormancy. Oecologia *172*, 937–947. .

Grousl, T., Ungelenk, S., Miller, S., Ho, C.-T., Khokhrina, M., Mayer, M.P., Bukau, B., and Mogk, A. (2018). A prion-like domain in Hsp42 drives chaperone-facilitated aggregation of misfolded proteins. J. Cell Biol. *217*, 1269–1285. .

Guidetti, R., Altiero, T., and Rebecchi, L. (2011). On dormancy strategies in tardigrades. J. Insect Physiol. *57*, 567–576. .

Haslbeck, M., Walke, S., Stromer, T., Ehrnsperger, M., White, H.E., Chen, S., Saibil, H.R., and Buchner, J. (1999). Hsp26: a temperature-regulated chaperone. EMBO J. *18*, 6744–6751. .

Haslbeck, M., Braun, N., Stromer, T., Richter, B., Model, N., Weinkauf, S., and Buchner, J. (2004). Hsp42 is the general small heat shock protein in the cytosol of Saccharomyces cerevisiae. EMBO J. *23*, 638–649. .

Haslbeck, M., Weinkauf, S., and Buchner, J. (2019). Small heat shock proteins: Simplicity meets complexity. J. Biol. Chem. *294*, 2121–2132. .

Herman, P.K., and Rine, J. (1997). Yeast spore germination: a requirement for Ras protein activity during re-entry into the cell cycle. EMBO J. *16*, 6171–6181. .

Ho, K.H., and Miller, J.J. (1978). Free proline content and sensitivity to desiccation and heat during yeast sporulation and spore germination. Can. J. Microbiol. *24*, 312–320. .

Holehouse, A.S., Ginell, G.M., Griffith, D., and Böke, E. (2021). Clustering of aromatic residues in prion-like domains can tune the formation, state, and organization of biomolecular condensates. Biochemistry *60*, 3566–3581. .

Huang, M., and Hull, C.M. (2017). Sporulation: how to survive on planet Earth (and beyond). Curr. Genet. *63*, 831–838. .

Iserman, C., Desroches Altamirano, C., Jegers, C., Friedrich, U., Zarin, T., Fritsch, A.W., Mittasch, M., Domingues, A., Hersemann, L., Jahnel, M., et al. (2020). Condensation of Ded1p Promotes a Translational Switch from Housekeeping to Stress Protein Production. Cell *181*, 818–831.e19. .

Janke, C., Magiera, M.M., Rathfelder, N., Taxis, C., Reber, S., Maekawa, H., Moreno-Borchart, A., Doenges, G., Schwob, E., Schiebel, E., et al. (2004). A versatile toolbox for PCR-based tagging of yeast genes: new fluorescent proteins, more markers and promoter substitution cassettes. Yeast *21*, 947–962. .

Jumper, J., Evans, R., Pritzel, A., Green, T., Figurnov, M., Ronneberger, O., Tunyasuvunakool, K., Bates, R., Žídek, A., Potapenko, A., et al. (2021). Highly accurate protein structure prediction with AlphaFold. Nature *596*, 583–589. .

Kane, S.M., and Roth, R. (1974). Carbohydrate metabolism during ascospore development in yeast. J. Bacteriol. *118*, 8–14. .

Kanshin, E., Kubiniok, P., Thattikota, Y., D'Amours, D., and Thibault, P. (2015). Phosphoproteome dynamics of Saccharomyces cerevisiae under heat shock and cold stress. Mol. Syst. Biol. *11*, 813. .

Kerr, C.H., Skinnider, M.A., Andrews, D.D.T., Madero, A.M., Chan, Q.W.T., Stacey, R.G., Stoynov, N., Jan, E., and Foster, L.J. (2020). Dynamic rewiring of the human interactome by interferon signaling. Genome Biol. *21*, 140. .

Lancaster, A.K., Nutter-Upham, A., Lindquist, S., and King, O.D. (2014). PLAAC: a web and command-line application to identify proteins with prion-like amino acid composition. Bioinformatics *30*, 2501–2502. .

Leducq, J.-B., Nielly-Thibault, L., Charron, G., Eberlein, C., Verta, J.-P., Samani, P., Sylvester, K., Hittinger, C.T., Bell, G., and Landry, C.R. (2016). Speciation driven by hybridization and chromosomal plasticity in a wild yeast. Nat Microbiol *1*, 15003. .

Liu, I.-C., Chiu, S.-W., Lee, H.-Y., and Leu, J.-Y. (2012). The histone deacetylase Hos2 forms an Hsp42-dependent cytoplasmic granule in quiescent yeast cells. Mol. Biol. Cell *23*, 1231–1242. .

Liu, Z., Zhang, S., Gu, J., Tong, Y., Li, Y., Gui, X., Long, H., Wang, C., Zhao, C., Lu, J., et al. (2020). Hsp27 chaperones FUS phase separation under the modulation of stress-induced phosphorylation. Nat. Struct. Mol. Biol. *27*, 363–372. .

Madshus, I.H. (1988). Regulation of intracellular pH in eukaryotic cells. Biochem. J *250*, 1–8. .

Martínez-Montañés, F., Casanovas, A., Sprenger, R.R., Topolska, M., Marshall, D.L., Moreno-Torres, M., Poad, B.L.J., Blanksby, S.J., Hermansson, M., Jensen, O.N., et al. (2020). Phosphoproteomic Analysis across the Yeast Life Cycle Reveals Control of Fatty Acyl Chain Length by Phosphorylation of the Fatty Acid Synthase Complex. Cell Reports *32*, 108024. https://doi.org/10.1016/j.celrep.2020.108024.

van Mierlo, G., Jansen, J.R.G., Wang, J., Poser, I., van Heeringen, S.J., and Vermeulen, M. (2021). Predicting protein condensate formation using machine learning. Cell Rep. *34*, 108705. .

Miesenböck, G., De Angelis, D.A., and Rothman, J.E. (1998). Visualizing secretion and synaptic transmission with pH-sensitive green fluorescent proteins. Nature *394*, 192–195. .

Miller, A.K., Brown, J.S., Enderling, H., Basanta, D., and Whelan, C.J. (2021). The Evolutionary Ecology of Dormancy in Nature and in Cancer. Frontiers in Ecology and Evolution *9*. https://doi.org/10.3389/fevo.2021.676802.

Mok, J., Kim, P.M., Lam, H.Y.K., Piccirillo, S., Zhou, X., Jeschke, G.R., Sheridan, D.L., Parker, S.A., Desai, V., Jwa, M., et al. (2010). Deciphering protein kinase specificity through large-scale analysis of yeast phosphorylation site motifs. Sci. Signal. *3*, ra12. .

Molines, A.T., Lemière, J., Gazzola, M., Steinmark, I.E., Edrington, C.H., Hsu, C.-T., Real-Calderon, P., Suhling, K., Goshima, G., Holt, L.J., et al. (2022). Physical properties of the cytoplasm modulate the rates of microtubule polymerization and depolymerization. Dev. Cell *57*, 466–479.e6. .

Mühlhofer, M., Peters, C., Kriehuber, T., Kreuzeder, M., Kazman, P., Rodina, N., Reif, B., Haslbeck, M., Weinkauf, S., and Buchner, J. (2021). Phosphorylation activates the yeast small heat shock protein Hsp26 by weakening domain contacts in the oligomer ensemble. Nat. Commun. *12*, 6697. .

Munder, M.C., Midtvedt, D., Franzmann, T., Nüske, E., Otto, O., Herbig, M., Ulbricht, E., Müller, P., Taubenberger, A., Maharana, S., et al. (2016). A pH-driven transition of the cytoplasm from a fluid- to a solid-like state promotes entry into dormancy. eLife *5*. https://doi.org/10.7554/elife.09347.

Narayanaswamy, R., Levy, M., Tsechansky, M., Stovall, G.M., O'Connell, J.D., Mirrielees, J., Ellington, A.D., and Marcotte, E.M. (2009). Widespread reorganization of metabolic enzymes into reversible assemblies upon nutrient starvation. Proc. Natl. Acad. Sci. U. S. A. *106*, 10147–10152. .

Neiman, A.M. (2011). Sporulation in the budding yeast Saccharomyces cerevisiae. Genetics *189*, 737–765. .

Oren, Y. (2022). Standing on the shoulders of microbes: How cancer biologists are expanding their view of hard-to-kill persister cells. Mol. Syst. Biol. *18*, e11168. .

Ortiz, S.C., Huang, M., and Hull, C.M. (2019). Spore Germination as a Target for Antifungal Therapeutics. Antimicrob. Agents Chemother. https://doi.org/ 10.1128/AAC.00994-19.

Parry, B.R., Surovtsev, I.V., Cabeen, M.T., O'Hern, C.S., Dufresne, E.R., and Jacobs-Wagner, C. (2014). The Bacterial Cytoplasm Has Glass-like Properties and Is Fluidized by Metabolic Activity. Cell *156*, 183–194. https://doi.org/10.1016/j.cell.2013.11.028.

Parsell, D.A., and Lindquist, S. (1993). The function of heat-shock proteins in stress tolerance: degradation and reactivation of damaged proteins. Annu. Rev. Genet. *27*, 437–496. .

Penfield, S. (2017). Seed dormancy and germination. Curr. Biol. *27*, R874–R878. .

Penfield, S. (2021). Water sensing in seeds by FLOE1 phase transitions. Dev. Cell *56*, 2140–2141. .

Perez-Riverol, Y., Bai, J., Bandla, C., García-Seisdedos, D., Hewapathirana, S., Kamatchinathan, S., Kundu, D.J., Prakash, A., Frericks-Zipper, A., Eisenacher, M., et al. (2022). The PRIDE database resources in 2022: a hub for mass spectrometry-based proteomics evidences. Nucleic Acids Res. *50*, D543–D552. .

Persson, L.B., Ambati, V.S., and Brandman, O. (2020). Cellular Control of Viscosity Counters Changes in Temperature and Energy Availability. Cell *183*, 1572–1585.e16. .

Petrovska, I., Nüske, E., Munder, M.C., Kulasegaran, G., Malinovska, L., Kroschwald, S., Richter, D., Fahmy, K., Gibson, K., Verbavatz, J.-M., et al. (2014). Filament formation by metabolic enzymes is a specific adaptation to an advanced state of cellular starvation. Elife *3*, e02409. .

Phan, T.G., and Croucher, P.I. (2020). The dormant cancer cell life cycle. Nat. Rev. Cancer *20*, 398–411. .

Plante, S., and Landry, C.R. (2020a). Closely related budding yeast species respond to different ecological signals for spore activation.

Plante, S., and Landry, C.R. (2020b). Purification of Yeast Spores to Investigate Their Dynamics of Activation. Current Protocols in Microbiology *59*. https://doi.org/10.1002/cpmc.123.

Plante, S., Normant, V., Ramos-Torres, K.M., and Labbé, S. (2017). Cell-surface copper transporters and superoxide dismutase 1 are essential for outgrowth during fungal spore germination. J. Biol. Chem. *292*, 11896–11914. .

Riback, J.A., Katanski, C.D., Kear-Scott, J.L., Pilipenko, E.V., Rojek, A.E., Sosnick, T.R., and Drummond, D.A. (2017). Stress-Triggered Phase Separation Is an Adaptive, Evolutionarily Tuned Response. Cell *168*, 1028–1040.e19. .

Schneider, C.A., Rasband, W.S., and Eliceiri, K.W. (2012). NIH Image to ImageJ: 25 years of image analysis. Nat. Methods *9*, 671–675. .

Schwanhäusser, B., Busse, D., Li, N., Dittmar, G., Schuchhardt, J., Wolf, J., Chen, W., and Selbach, M. (2011). Global quantification of mammalian gene expression control. Nature *473*, 337–342. .

Shevchenko, A., Wilm, M., Vorm, O., and Mann, M. (1996). Mass Spectrometric Sequencing of Proteins from Silver-Stained Polyacrylamide Gels. Analytical Chemistry *68*, 850–858. https://doi.org/10.1021/ac950914h.

Silva, A., Cavero, S., Begley, V., Solé, C., Böttcher, R., Chávez, S., Posas, F., and de Nadal, E. (2017). Regulation of transcription elongation in response to osmostress. PLOS Genetics *13*, e1007090. https://doi.org/10.1371/journal.pgen.1007090.

Smith, P.K., Krohn, R.I., Hermanson, G.T., Mallia, A.K., Gartner, F.H., Provenzano, M.D., Fujimoto, E.K., Goeke, N.M., Olson, B.J., and Klenk, D.C. (1985). Measurement of protein using bicinchoninic acid. Analytical Biochemistry *150*, 76–85. https://doi.org/10.1016/0003-2697(85)90442-7.

Sprouffske, K., and Wagner, A. (2016). Growthcurver: an R package for obtaining interpretable metrics from microbial growth curves. BMC Bioinformatics *17*, 172. .

Stoddard, P.R., Lynch, E.M., Farrell, D.P., Dosey, A.M., DiMaio, F., Williams, T.A., Kollman, J.M., Murray, A.W., and Garner, E.C. (2020). Polymerization in the actin ATPase clan regulates hexokinase activity in yeast. Science *367*, 1039–1042. .

Swaney, D.L., Beltrao, P., Starita, L., Guo, A., Rush, J., Fields, S., Krogan, N.J., and Villén, J. (2013). Global analysis of phosphorylation and ubiquitylation cross-talk in protein degradation. Nat. Methods *10*, 676–682. .

Triandafillou, C.G., and Drummond, D.A. (2020). Live Cell Measurement of the Intracellular pH of Yeast by Flow Cytometry Using a Genetically-Encoded Fluorescent Reporter. Bio Protoc *10*, e3653. .

Triandafillou, C.G., Katanski, C.D., Dinner, A.R., and Drummond, D.A. (2020). Transient intracellular acidification regulates the core transcriptional heat shock response. Elife *9*. https://doi.org/10.7554/eLife.54880.

Vlaar, L.E., Bertran, A., Rahimi, M., Dong, L., Kammenga, J.E., Helder, J., Goverse, A., and Bouwmeester, H.J. (2021). On the role of dauer in the adaptation of nematodes to a parasitic lifestyle. Parasit. Vectors *14*, 554. .

Wallace, E.W.J., Kear-Scott, J.L., Pilipenko, E.V., Schwartz, M.H., Laskowski, P.R., Rojek, A.E., Katanski, C.D., Riback, J.A., Dion, M.F., Franks, A.M., et al. (2015). Reversible, Specific, Active Aggregates of Endogenous Proteins Assemble upon Heat Stress. Cell *162*, 1286–1298. .

Wippich, F., Bodenmiller, B., Trajkovska, M.G., Wanka, S., Aebersold, R., and Pelkmans, L. (2013). Dual specificity kinase DYRK3 couples stress granule condensation/dissolution to mTORC1 signaling. Cell *152*, 791–805. .

Wyatt, T.T., Wösten, H.A.B., and Dijksterhuis, J. (2013). Fungal spores for dispersion in space and time. Adv. Appl. Microbiol. *85*, 43–91. .

Yoo, H., Bard, J.A.M., Pilipenko, E.V., and Drummond, D.A. (2022). Chaperones directly and efficiently disperse stress-triggered biomolecular condensates. Mol. Cell *82*, 741–755.e11. .

Figures and legends

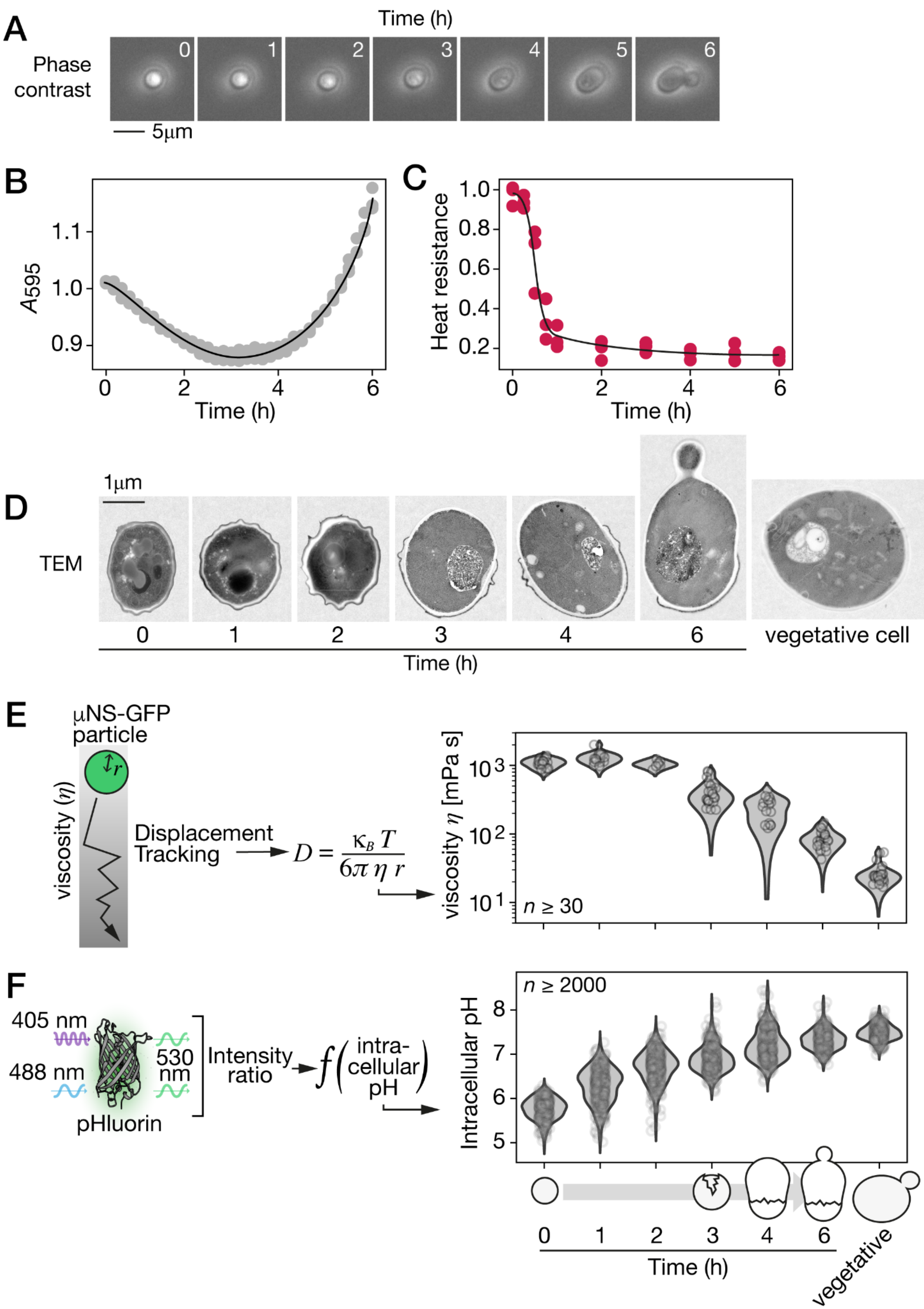
A
Time (h)
Phase contrast
0
1
2
3
4
5
6
5μm
B
A595
Time (h)
C
Heat resistance
Time (h)
D
1μm
TEM
0
1
2
3
4
6
vegetative cell
Time (h)
E
μNS-GFP particle
viscosity (η)
Displacement Tracking
$D = \frac{\kappa_B T}{6\pi \eta r}$
viscosity η [mPa s]
n ≥ 30
F
405 nm
488 nm
530 nm
pHluorin
Intensity ratio
f(intra-cellular pH)
Intracellular pH
n ≥ 2000
Time (h)
vegetative

Figure 1 - The cytoplasm of dormant cells displays high viscosity and is an acidic environment.

A) Representative phase-contrast microscopic images of a spore at the indicated time after exposure to rich media, which activates germination. Scale bar represents 5 µm.
B) Optical density (A_{595}) and C) heat resistance of pure spore cultures through time after exposure to rich media. Heat resistance is the ratio of growth after a heat shock at 55˚C for 10 minutes to growth without heat treatment. Experiments were performed in triplicate and values for individual replicates are shown.
D) Representative transmission electron microscopic (TEM) images of spores at the indicated time after exposure to rich media, and of a vegetatively growing yeast cell (vegetative). The scale bar represents 1 µm. See Figure S1A for more examples.
E) Left, effective viscosity (η) was estimated from the displacement constant of a single µNS-GFP particle of radius r using the Stock-Einstein relation. Right, single cell measurement of viscosity at the indicated time points after exposure to rich media, and in vegetatively growing yeast cells. Results of tracking of 30 to 35 particles in 30 to 32 cells at each time point.
F) Left, pHluorin is excited with a 405 nm and 488 nm laser, and the ratio of fluorescence varies as a function of intracellular pH. Right, intracellular pH measured at the indicated time point after germination induction, and in exponentially growing cells. Measurements in at least 2000 cells are shown at each time point.

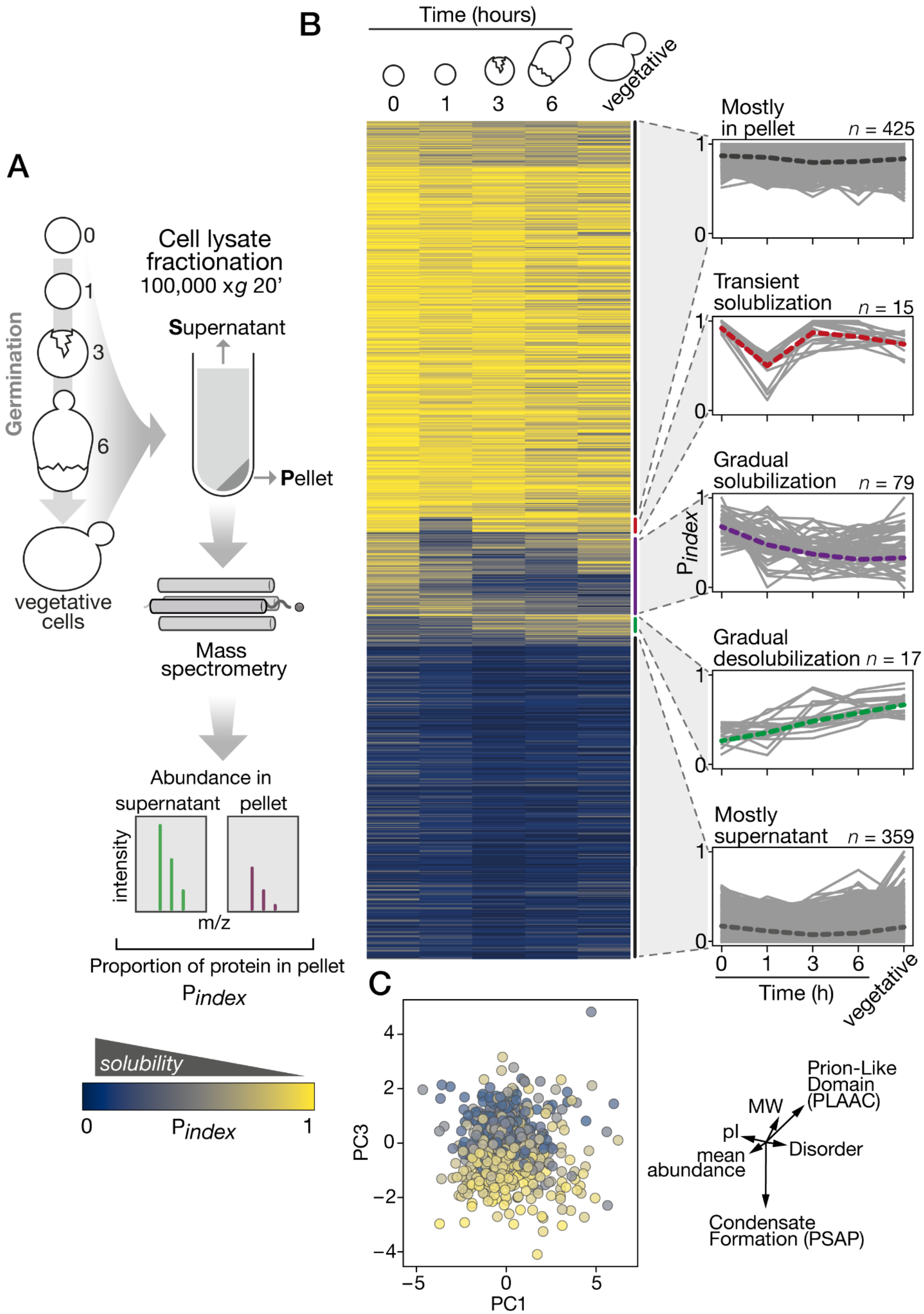
A
Germination
0
1
3
6
vegetative cells
Cell lysate fractionation
100,000 xg 20'
Supernatant
Pellet
Mass spectrometry
Abundance in
supernatant pellet
intensity
m/z
Proportion of protein in pellet
Pindex
solubility
0
Pindex
1
B
Time (hours)
0
1
3
6
vegetative
Mostly in pellet n = 425
Transient solubilization n = 15
Gradual solubilization n = 79
Gradual desolubilization n = 17
Mostly supernatant n = 359
Pindex
Time (h)
C
PC3
PC1
Prion-Like Domain (PLAAC)
MW
pI
mean abundance
Disorder
Condensate Formation (PSAP)

Figure 2 - Proteome wide change in protein solubility during germination.
A) Solubility measurement by LC-MS/MS estimates the proportion of each protein in the pellet (P_{index}) at each major time-point sampled during germination. The experiment was performed in triplicate for all timepoints.
B) Right, P_{index} values in the course of germination show, from top to bottom, proteins consistently found in the pellet, that transiently solubilize, that gradually solubilize, that gradually accumulate in the pellet, and that are consistently found in the supernatant. Left, individual P_{index} trajectories for each cluster determined by hierarchical clustering. The dotted line is the median trajectory for each cluster.
C) Left, PCA analysis of multivariate distribution for all proteins, dots are colored according to mean P_{index}. Right, vectors indicate the strength and direction of the contribution of each variable to the distribution; sequence-based estimation of molecular weight (MW) and isoelectric point (pI); mean abundance measured from our proteomic data; Prion-like amino acid composition (PLAAC) prediction score; analysis and prediction score of phase separation (PSAP); sequence-based prediction of disorder (Metapredict). See Figure S2 for additional details.

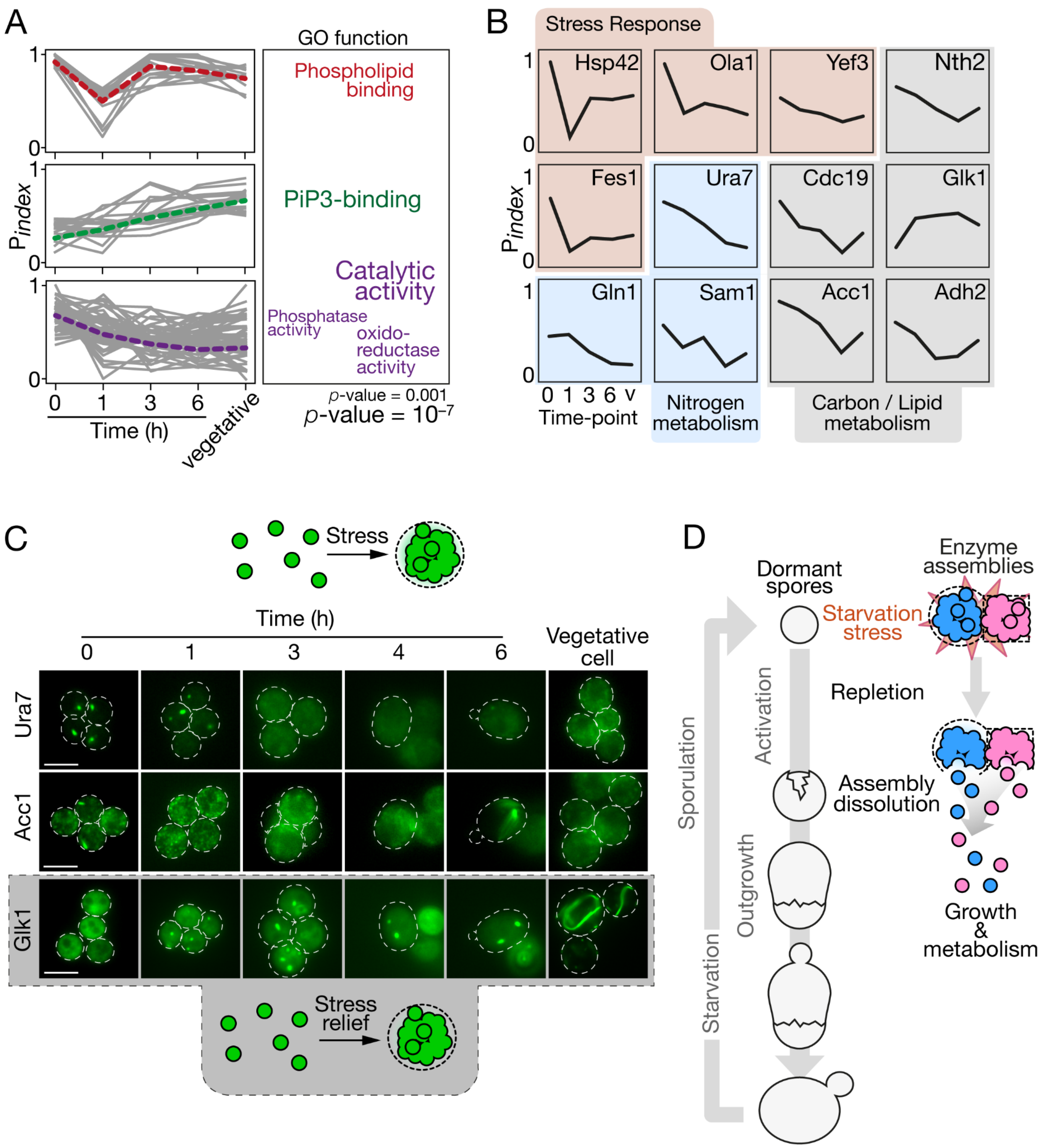

Figure 3 - Solubility changes reflect metabolism activation and stress relief during germination.

A) Enrichment for gene ontology terms in each dynamically changing solubility cluster. Red, transiently solubilizing cluster; Green, gradual desolubilization cluster; Purple, gradual solubilization cluster. P-values are from a hypergeometric test. Font size scales with -log10 (p-value). p-values are shown at bottom right for scale.

B) Individual P_{index} trajectory for representative proteins through germination. Proteins are clustered by function; Red, stress response proteins; Blue, Nitrogen metabolism proteins; Gray, Lipid and carbon metabolism proteins.
C) Representative fluorescence microscopic images of spores expressing the indicated proteins tagged with GFP during germination. Top, Acetyl-CoA carboxylase Acc1 (Lipid biosynthesis) and CTP synthase Ura7 (pyrimidines synthesis) have similar comportement as they both condense upon stress; bottom, Glucokinase Glk1 (glycolysis) behaves in an opposite manner; it aggregate upon nutrient repletion. Dotted lines indicate cell contour determined by brightfield images. Scale bars represent 5μm.
D) Schematics highlighting effects on protein solubility of nutrient starvation and repletion during sporulation and germination, respectively.

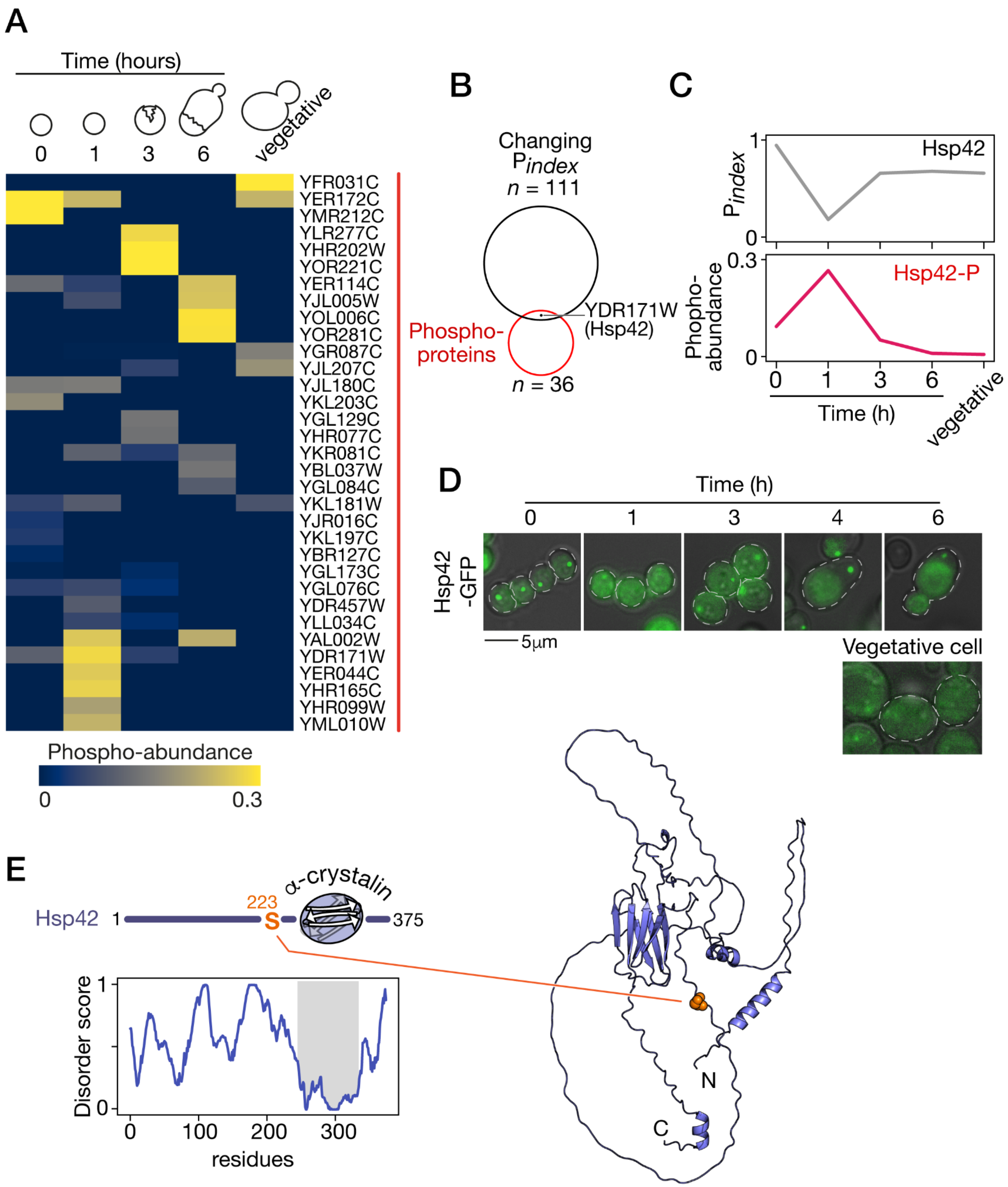

Figure 4 - Hsp42 phosphorylation at S223 is synchronized with its transient solubilization.

A) Relative abundance of the 36 phosphoproteins to the total abundance of each protein through germination.

B) Hsp42 is phosphorylated during germination and changes solubility. See Figure S3 for additional information.
C) Hsp42 is the only protein with dynamic solubility profile during germination that correlates with its dynamic phosphorylation at S223.
D) Representative fluorescence microscopic images of spores expressing Hsp42-GFP at the indicated time after the induction of germination. Dotted lines represent cell contour. Scale bar represents 5μm.
E) Left, Disorder profile of Hsp42, predicted by Metapredict, shows the predicted structured ACD domain, and flanking disordered N- and C-terminal region. Right, predictedHsp42 structure. The S223 highlighted in orange is located in a disordered region.

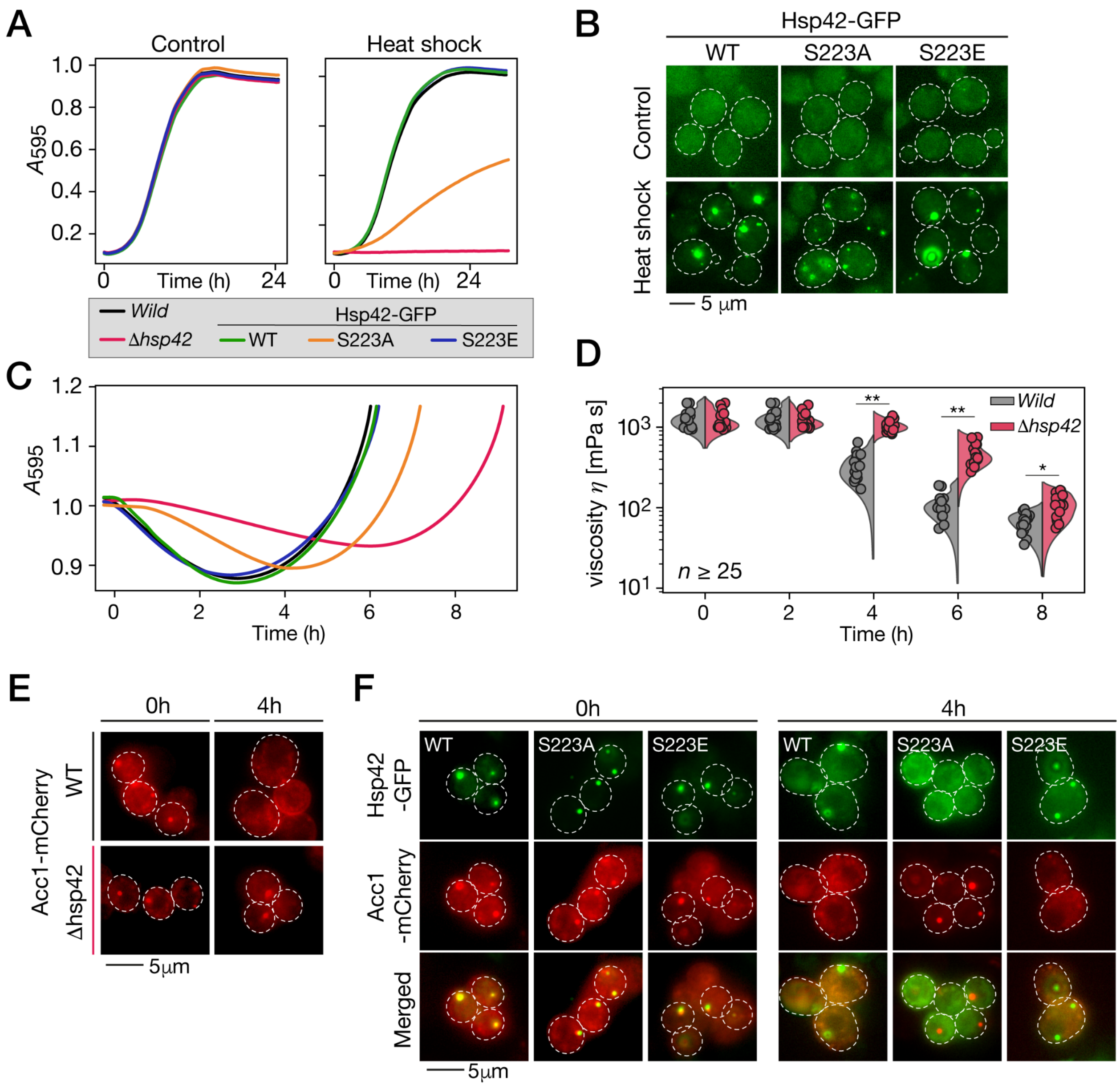

Figure 5 - Active and phosphorylated Hsp42 is required for normal germination dynamics.

A) Growth curves of vegetative cells of the indicated strains after a heat shock (right) or a mock treatment at control temperature (left). Shown are the data of one replicate representative of three independent experiments. The non-phosphorylatable Hsp42 at S223 shows intermediate heat-shock resistance between the WT (and phosphomimetic) and *HSP42* deleted cells. This confirms that the phosphorylation of Hsp42 at this site is important for its function.

B) Fluorescence microscopic images of WT or mutant Hsp42-GFP expressing cells, in control conditions (top) or after a heat shock (bottom). Dotted lines represent cell

contour. Scale bar represents 5 µm. The non-phosphorylatable Hsp42 at S223 shows smaller and fainter aggregates in cells following heat shock at 50˚C for 10 minutes compared to WT and phosphomimetic.
C) Optical density measurements of pure spore culture following exposure to germination conditions. Lines are colored according to the strain like in A)
D) Effective viscosity measured in wild type (grey) or ΔHsp42 spores at the indicated time after the induction of germination. At each time point for each strain, 25 to 35 particles, corresponding to the same number of cells, were tracked. Kruskal-Wallis test, ** indicates p-value < 0.0001, * indicates p-value < 0.01.
E) Fluorescence microscopy images of wild type (top) or ΔHsp42 spores expressing Acc1-mCherry at the indicated time after exposure to germination conditions. Scale bar represents 5µm.
F) Fluorescence microscopy images of spores expressing either WT or mutants Hsp42-GFP and Acc1-mCherry at the indicated time after exposure to germination conditions. Dotted lines represent cell contour. Scale bar represents 5 µm. Expression of non-phosphorylatable Hsp42 at S223 shows delay in Acc1 foci dissolution in spores.

Supplemental informations

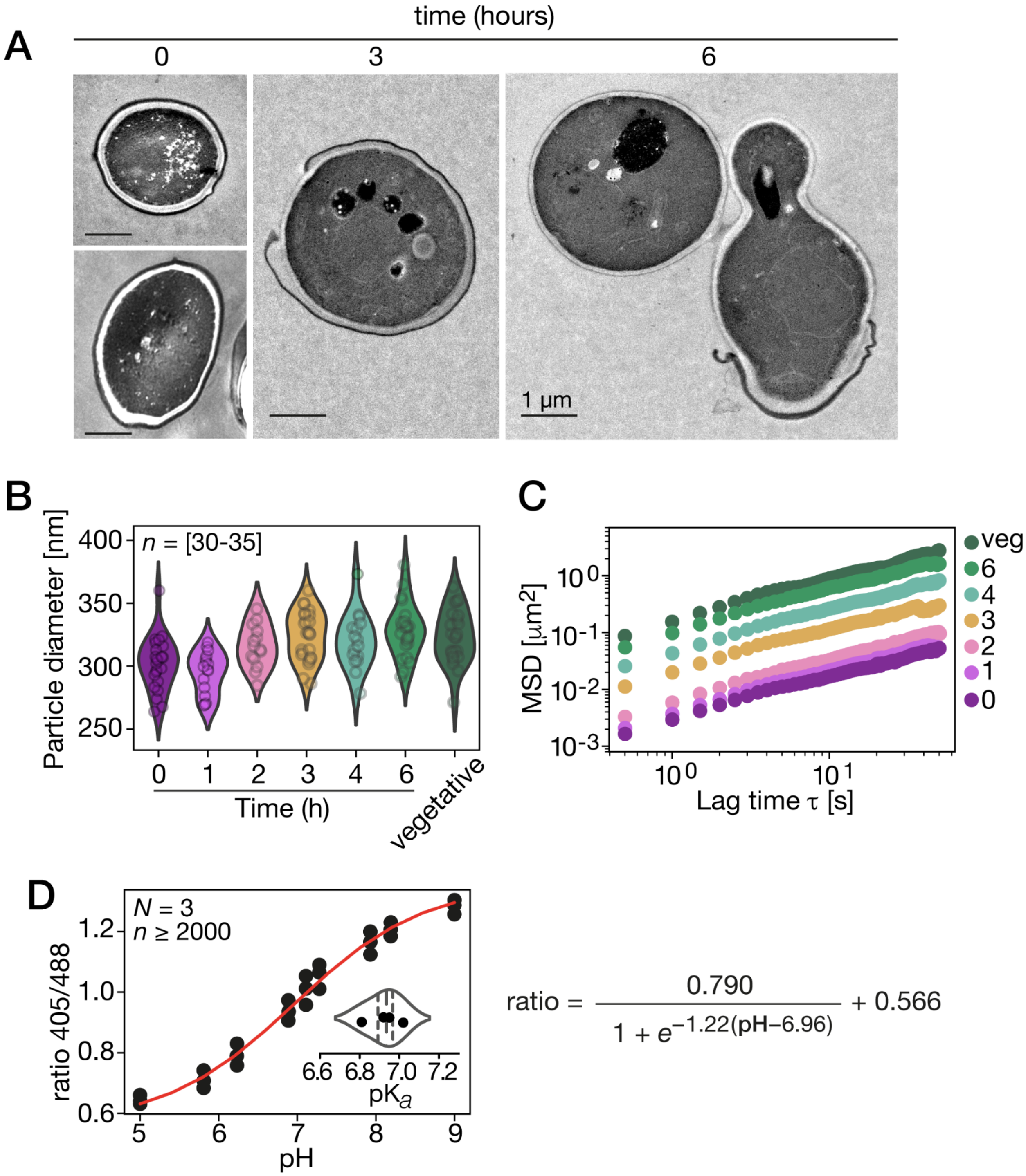

Figure S1 - µNS-GFP particle size and Mean square displacement (MSD) during germination; calibration curve of pHluorin emission ratio, related to figure 1.

A) Transmission electron microscopy images of spores at the indicated time after exposure to rich medium. Scale bar represents 1 μm.
B) Size of individual particles tracked at each time point during germination and in vegetatively growing cells. At least 30 particle were tracked at each time point
C) Mean square displacement (MSD) for each time point. Obtained from combining the 30 to 35 tracked particles. Points are colored according to the time point.
D) Calibration curves for pH determination. The experiment was done on three technical replicates. At each pH point, at least 2000 events were recorded. Inset, plot of the measured pKa of pHluorin for each replicate. Right, logistic function fitted to the data that was used to estimate intracellular pH (Figure 1F).

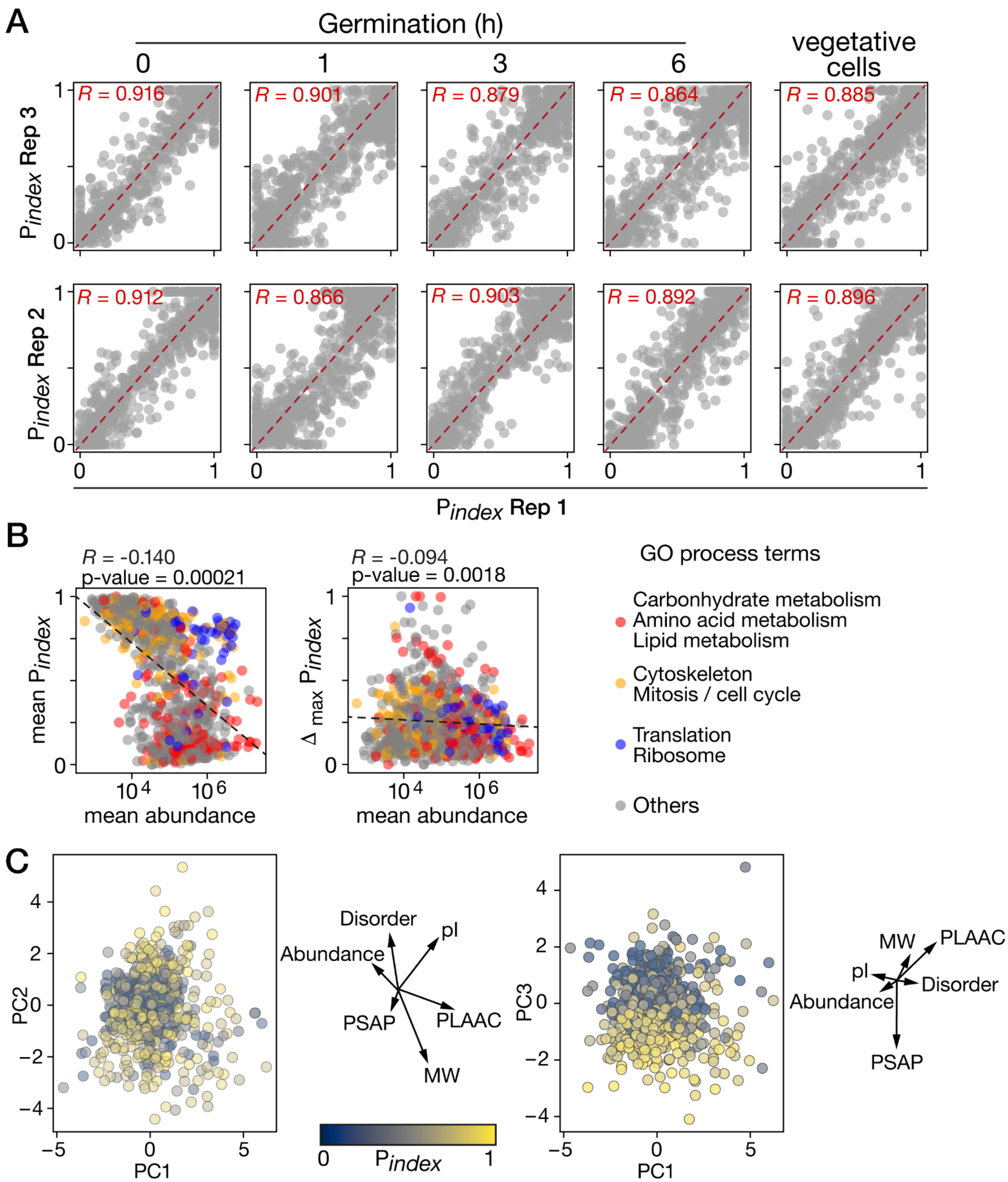

Figure S2 - Pindex correlation between replicates, influence of protein abundance on solubility measurements, and contribution of protein properties on P_{index} distribution. Related to Figure 2.

A) P_{index} values are plotted against other replicates. Pearson's correlation coefficients are indicated on each graph. For all correlations, p-value < 0.0001.
B) Mean of the absolute abundance estimated from mass spectrometry data during germination is plotted against mean Pindex values (left), or the maximal Pindex variation (right, $\Delta_{max}P_{index}$) of each protein. Points are colored depending on the GO function term. Pearson's correlation coefficient with the log10-transformed abundance values are shown with the corresponding p-values.
C) PCA analysis of protein properties. Protein distribution across PC1 vs PC2 (left) and PC1 vs PC3 (right). Dots are colors according to the mean P_{index} value. Beside the graph is the vector representation of the contribution of each protein properties to each principal component plotted.

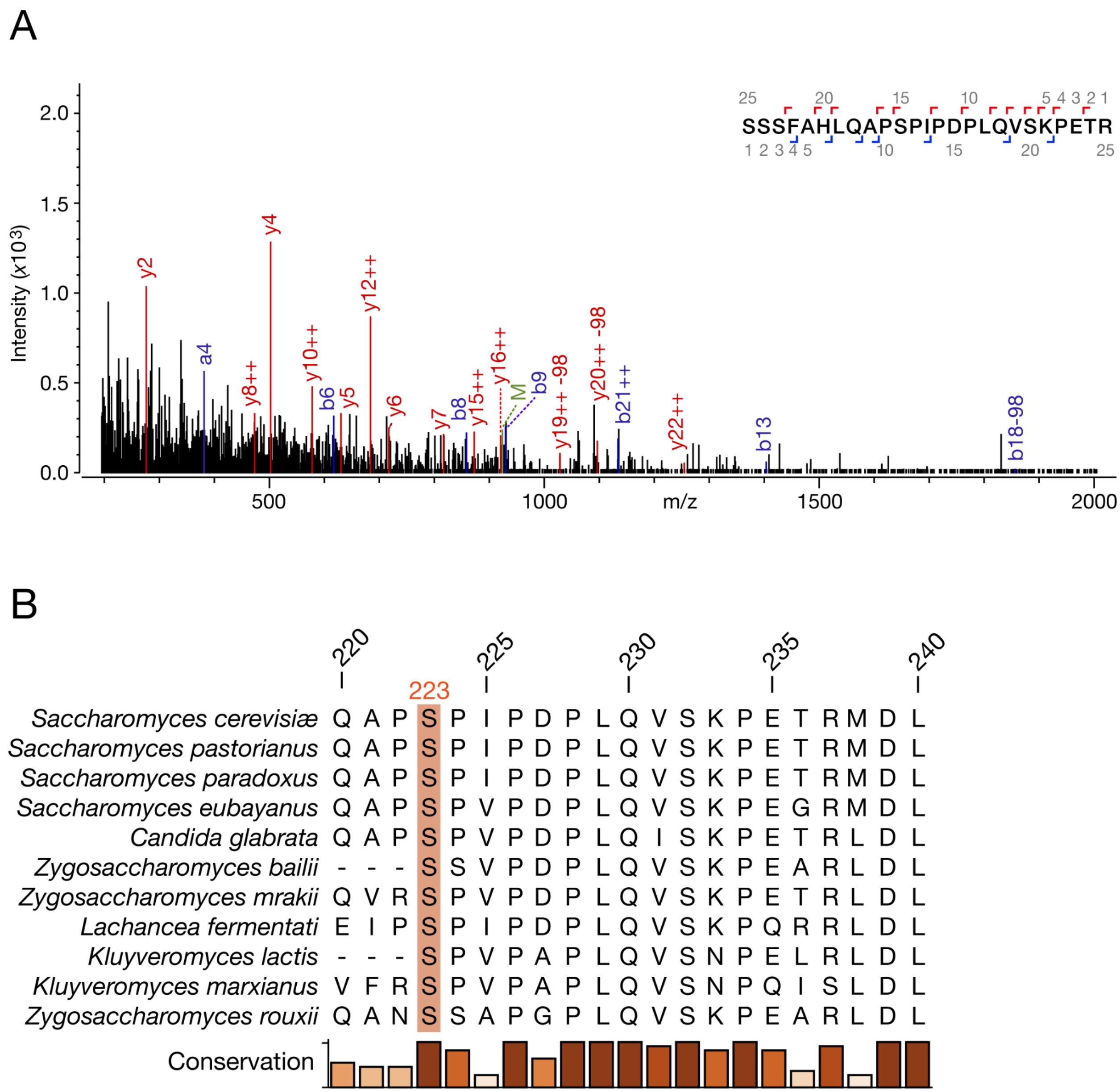

Figure S3 - Hsp42 S223 phosphorylation, related to figure 4.

A) MS spectra example of phosphorylated S223 peptide on Hsp42.

B) Multiple Sequence Alignment of Hsp42 orthologs. Numbers on top refer to residue position in the *S. cerevisiae* protein. S223 is underlined in orange. Relative conservation is shown with the bars at the bottom. Only a small portion of the sequences are shown.

Table S1
Primers used in this study

Name	Sequence	Description
Site-directed mutagenisis on Hsp42		
CLO5-97	AAGCGCCTGCCCCAATACC	HSP42 S223A up
CLO5-98	GGTATTGGGGCAGGCGCTT	HSP42 S223A down
CLO6-1	AAGCGCCTGAACCAATACC	HSP42 S223E up
CLO6-2	GGTATTGGTTCAGGCGCTT	HSP42 S223E down
HSP42 deletion		
CLO6-5	GTCCATATCCCACACAAATTAAGATCATACCAAGCCGAAGCcagctgaagcttcgtacgc	Forward amplification of lox-KANMX-lox cassette (pUG6) for HSP42 (YDR171W) KO
CLO6-6	CATTCGTTGTATGATTTTTGTGTGGTTGACAGATATTCTGCCGgcataggccactagtggatctg	Reverse amplification of lox-KANMX-lox cassette (pUG6) for HSP42 (YDR171W) KO
Rescue Hsp42 expression		
CLO6-7	CCATATCCCACACAAATTAAGATCATACCAAGCCGAAGCAATGAGTTTTTATCAACCATCCC	Forward amplification of 40pb promotor + Hsp42 for integration
CLO6-8	attcttcacctttagaATTTTCTACCGTAGGGTTGGGATTTTC	Reverse amplification of

		Hsp42 no stop fused to EGFP
CLO6-11	GCACCACAAAATAAATAATCTGAACtctaaaggtgaagaattattc	Forward amplification of Hsp42 for cloning in pYM25
CLO6-12	CGTACACACGTAAATATATTCgcagtatagcgaccagcattc	Reverse amplification of pYM25 for cloning of Hsp42
CLO6-9	CCCTACGGTAGAAAATtctaaaggtgaagaattattcactgg	Forward amplification EGFP (pYM25) fused to Hsp42
C-terminal tagging at native genomic loci		
CLOP194-B10	CTAAACCCTGTTGGTGTTCCAAATGATGACCACCATCACgtgagcaagggcgaggagg	forward to tag ACC1 (YNR016C) (cerevisiae) with mCherry
CLOP194-E10	GGTAAAAAGTAAAAGAGAAACAGAAGGGCAACTTGAATGgtggatctgatatcatcgatg	reverse to tag ACC1 (YNR016C) cerevisiae (pYM27, pBS35)
CLOP258-A3	TATCTACCGATGATAAAGAAAAATTGTTGAAGACTTTGAAAtctaaaggtgaagaattattc	F to tag ACC1 (YNR016C) with eGFP (pKT127)
CLOP258-B3	GATGATGGAAGCGCTCAAACAGATCCTTCAGAGTACTTGGcagtatagcgaccagcattc	R to tag ACC1 (YNR016C) with eGFP (pKT127)
CLOP258-E3	GTAAGTACGATCTTGAGGCCGGCGAAAACAAATTCAACTTTtctaaaggtgaagaattattc	F to tag URA7 (YBL039C) with eGFP (pKT127)
CLOP258-F3	GTTCATGTCATCACCTACAATCGACTTCAACTCGAAGAGTgcagtatagcgaccagcattc	R to tag URA7 (YBL039C) with

		eGFP (pKT127)
CLOP258-A4	GGTTCCGGAGTGGGTGCCGCCTTGTGTGCGCTTGTAGCAtctaaaggtgaagaattattc	F to tag GLK1 (YCL040W) with eGFP (pKT127)
CLOP258-B4	GGAGAGAAGATGGTAAGTACGGTGGGATACGTACACAAACgcagtatagcgaccagcattc	R to tag GLK1 (YCL040W) with eGFP (pKT127)
CLOP273-D2	GATGATGGAAGCGCTCAAACAGATCCTTCAGAGTACTTGGGGACCTAGACTTCAGGTTGTC	R to tag ACC1 (YNR016C) with eGFP (pYM25)
CLOP273-F2	GTTCATGTCATCACCTACAATCGACTTCAACTCGAAGAGTGGACCTAGACTTCAGGTTGTC	R to tag URA7 (YBL039C) with eGFP (pYM25)
CLOP273-H2	GGAGAGAAGATGGTAAGTACGGTGGGATACGTACACAAACGGACCTAGACTTCAGGTTGTC	R to tag GLK1 (YCL040W) with eGFP (pYM25)
CLO6-10	CGCAGCTAATGCGAAACAAAGAAATGAAGCATATACCATTCGcgatgaattcgagctcgtttaaactgg	Reverse amplification EGFP-TERM-KAN MX cassette (pYM25) to integrate at HSP42 (YDR171W) loci
Molecular probes (µNS and pHluorin)		
CLOP228-A2	CAATGTATCTTAccagcttttgttccctttagtgaggg	Forward amplification pRS vector
CLOP228-B2	TTAGTCGATGCCcccggtacccaattcgccctatag	reverse amplification pRS vector + SOD1p (YJR104C)
CLOP228-D2	gggtaccgggGGCATCGACTAAAATTGCATCGTTG	F sod1 (YJR104C) prom to clone in pRS

CLOP228-E2	**gaatgaagccatCGATTTGTATTTTATTTACGTGC**	**R sod1 (YJR104C) prom to clone upstream ¬µNS**
CLOP228-H2	**aaatacaaatcgATGGCTTCATTCAAGGGATTCTCCGC**	**Forward µNS downstream sod1p (YJR104C)**
CLOP228-B3	**aacaaaagctggTAAGATACATTGATGAGTTTGGAC**	**rev µNS-EGFP**
CLOP239-A3	**gggtaccgggCTCGCTGAACTTGTCCTTACCGACGG**	**F to clone -850 sod1_cer promotor in pRS**
CLOP239-B3	**gaatgaagccatTATAAATTAATTATGTTTTATTTGTTTGCGCGATTGC**	**R to clone sod1_cer prom (from -1) upstream muNS**
CLOP239-C3	**ttaatttataATGGCTTCATTCAAGGGATTCTCCGC**	**F to clone muNS downstream -1 sod1_cer**
CLOP239-D3	**GTTCAGCGAGcccggtacccaattcgccctatag**	**R to amplify pRS with -850 sod1_cer**
CLOP247-H6	**CCCAGTATTCTTAACCCAACTGCACAGAACAAAAACCTGCagcttgcctcgtccccgccggg**	**Forward to integrate HYG_sod1P_muNS_EGFP (pYM25) at Ura3 (YEL021W) locus**
CLOP247-A7	**GTGAGTTTAGTATACATGCATTTACTTATAATACAGTTTTttacttgtacagctcgtccatgc**	**reverse to integrate HYG_sod1P_muNS_EGFP (pYM25) at Ura3 (YEL021W) locus**

CLOP249-A2	**GACGCTCGAAGccagcttttgttccctttagtgaggg**	**forward to amplify pYM25 for gibson cloning with sfpHluorin**
CLOP249-B2	**ctttgctcatTATAAATTAATTATGTTTTATTTGTTTGCGCGATTGC**	**reverse to amplify pYM25_sod1_promoter to clone sfpHluorin downstream promoter**
CLOP249-C2	**CATAATTAATTTATAatgagcaaaggagaagaacttttc**	**forward to amplify sfpHluorin to clone downstream sod1 promoter**
CLOP249-D2	**AACAAAAGCTGGcttcgagcgtcccaaaaccttc**	**reverse to amplify sfpHluorin to clone in pRS**
CLOP249-G2	**GTGAGTTTAGTATACATGCATTTACTTATAATACAGTTTTcttcgagcgtcccaaaaccttc**	**reverse to integrate HYG_sod1P_sfpHluorin (pYM25) at Ura3 (YEL021W) locus**
CLOP253-C6	**CATGAAATTGCCCAGTATTCTTAACCCAACTGCcatttgcatccatacattttgatggcc**	**Forw integration pHluorin to URA3 (YEL021W) locus**
CLOP253-F6	**GTTTAGTATACATGCATTTACTTATAATACAGttatttgtagagctcatccatgccatg**	**Rev integration pHluorin to URA3 (YEL021W) locus**
Validation and sequencing		
CLOP256-C9	**GTTCTGGAAGGTTCGCGAATTG**	**Forward KO check**
CLOP256-	**ctgctcgcaggtctgcagcgagg**	**Reverse KO check**

D9		
CLOP250-D7	**GTTTAGCTGTAACTATGTTGCGG**	**SOD1 prom -100 for seq**
CLOP250-E7	**ccttttcggttagagcggatgtgg**	**CYC1 term +100 for seq**
CLOP258-C4	**CGTGGTACCCTGCTTCAGTGGACC**	**oligo C ACC1 (YNR016C)**
CLOP258-E4	**GGTAAGGACGACACTGGAAAGCG**	**oligo C URA7 (YBL039C)**
CLOP258-G4	**GTGAAGTCGAGATCGGTTGTGATG**	**oligo C GLK1 (YCL040W)**

Table S2

Pindex values at indicated time-point during germination and in vegetatively growing cells.

Protein	Pindex				
Systematic name	0h	1h	3h	6h	vegetative cells
CON__P00761	0.44649274	0.31128444	0.40430669	0.48123797	0.555981157
CON__P08779	0.70775555	0.29725873	0.49761323	0.4333803	0.734509032
CON__P35527	0.60567557	0.2844409	0.41124666	0.37224188	0.529706682
CON__P35908v2	0.50507366	0.34537628	0.41173599	0.41876572	0.382999348
CON__Q04695	0.86379046	0.3675856	0.31372998	0.27394323	0.643764902
YAL003W	0.33483348	0.25533162	0.31925034	0.46049299	0.315911422
YAL005C	0.21945126	0.18832197	0.18530921	0.64456277	0.200656213
YAL012W	0.04410389	0.07951884	0.03860619	0.06325469	0.069915642
YAL016W	0.61410372	0.37593279	0.244234	0.25185204	0.253032038
YAL025C	1	0.52454417	1	0.98902062	0.834010926
YAL035W	0.91236418	0.8844249	0.85525553	0.86436319	0.824732227
YAL038W	0.74825732	0.41552458	0.40214569	0.13089211	0.399792677
YAL043C	0.99390408	1	0.94543868	0.96774365	0.889246444
YAL049C	0.00773975	0.04387666	0.00935912	0.03131348	0.071512226
YAL054C	0.56520666	0.50980753	0.4453242	0.2928999	0.686748634
YAL060W	0.04165426	0.15037505	0.05499783	0.09453735	0.084386059
YAR002C-A	0.89168735	0.80260029	1	1	0.990273682
YAR007C	0	0.04605261	0.10444699	0.113771	0.101953922
YAR015W	0.09982522	0.07635914	0.03417635	0.05635284	0.063844928
YBL004W	1	0.91957195	0.97551014	0.99046252	0.98306422
YBL015W	0.43121976	0.41367719	0.50386908	0.58694377	0.731044191

YBL017C	0.98040161	0.88440738	1	0.95482469	1
YBL024W	0.132439	0.15451424	0.01047809	0.06469429	0.028753854
YBL026W	0.87085761	0.47935758	0.48813462	0.48124558	0.576804795
YBL036C	0.0053118	0.04215186	0	0.02890359	0.108612113
YBL039C	0.78178556	0.6121169	0.36433411	0.15088733	0.144611002
YBL041W	0.1711052	0.23363467	0.06114067	0.0501647	0.11204643
YBL045C	0.76593793	0.79842009	0.82507854	0.80077656	0.814597956
YBL050W	0.79281123	0.65446347	0.86645521	0.9134249	0.975061344
YBL056W	0.59008016	0.655708	0	0.14929928	0
YBL058W	0.11310906	0.06076359	0	0.05599082	0.038200317
YBL064C	0.37294764	0.30036821	0.18090971	0.1874285	0.316348617
YBL075C	0.44535642	0.26091698	0.25190948	0.23598042	0.940606368
YBL076C	0.38199256	0.20015304	0.10344669	0.13792019	0.259505008
YBL092W	0.87436142	0.91707997	0.84121471	0.7651759	0.600270001
YBL099W	0.77069855	0.69246024	0.65218988	0.6076221	0.745423818
YBR001C	0.79575347	0.54598393	0.30757916	0.19451316	0.373884086
YBR011C	0.09657142	0.11757775	0.03669902	0.06265643	0.050322253
YBR015C	1	0.85779481	0.85514825	0.86483231	0.819181518
YBR025C	0.86472609	0.43926287	0.49026698	0.434375	0.357911999
YBR039W	0.94846757	0.94012684	0.96565205	0.91303578	0.991814674
YBR078W	0.26800799	0.30202208	0.52070068	0.8287967	0.904737272
YBR079C	0.95722376	0.8242318	0.88905626	0.80776128	0.80638378
YBR084W	0.85919524	0.90265676	0.97753366	0.90068394	0.842040317
YBR087W	1	1	1	0.89758438	0.950009968
YBR088C	0.01215203	0.0571025	0.01165576	0.00739966	0.042578745
YBR089C-A	0.60183628	0.62280786	0.52107595	0.56676699	0.369050091
YBR094W	0.24925825	0.37053217	0.03683753	0.25924149	0.087664834

YBR101C	0.6982609	0.58589689	0.30875016	0.27611464	0.186070032
YBR106W	0.91998997	0.91136652	1	1	1
YBR109C	0.53232225	0.66007706	0.43385648	0.43113022	0.342924176
YBR111C	0.30256508	0.26576518	0.07293678	0.05570606	0.10530896
YBR112C	0.71609689	0.75678188	0.20154218	0.04675914	0
YBR115C	0.0404644	0.02504774	0	0.03226828	0.018373298
YBR121C	0.31004777	0.1134969	0.09001346	0.16318818	0.168230788
YBR126C	0.16335842	0.12090812	0.13824235	0.10812091	0.272744483
YBR127C	0.84346454	0.83179217	0.79369736	0.74116963	0.796229867
YBR140C	0.96617781	0.97814179	1	1	1
YBR143C	0.69214767	0.58892871	0.51878972	0.66689485	0.627459756
YBR146W	1	0.83727271	1	1	0.666625786
YBR149W	0.04474086	0.05450444	0.02237537	0.02270145	0.048774991
YBR154C	0.62033293	0.75367432	0.71126735	0.60614446	0.675568947
YBR164C	0.9433279	0.76696415	0	0.58673301	0.564964399
YBR166C	1	0.9804613	0.86359633	0.79183028	1
YBR191W	0.90298831	0.93256618	0.89264192	0.77210022	0.749048561
YBR196C	0.05034515	0.11264977	0.02563034	0.05352399	0.083057298
YBR198C	1	0.78852505	0.78827557	0.90246404	1
YBR218C	0.50530186	0.43231662	0.29287456	0.44747305	0.514518342
YBR221C	0.78762334	0.75811184	0.85218671	0.87814685	0.961489859
YBR222C	0.02759917	0.12153594	0.05311911	0.12923374	0.491005355
YBR245C	1	0.81437219	0.98689055	0.71507906	0.729532123
YBR247C	0.92357562	0.66617749	0.5605413	0.76544947	0.851108167
YBR248C	0.0240767	0.08169108	0	0.01377634	0.03855732
YBR249C	0.59006642	0.29710993	0.23118736	0.37949854	0.294959481
YBR256C	0	0	0	0	0

YBR263W	0.6995731	0.82468481	0.74464549	0.76814972	0.8524565
YBR286W	0.07928795	0.14276605	0.0554474	0.08136698	0
YCL011C	0.37177429	0.36829098	0.38231401	0.28194134	0.201479866
YCL017C	0.9025791	0.73676915	0.80301877	0.74418001	0.546172509
YCL030C	0.46969892	0.07795779	0.19360007	0.21306047	0.336685382
YCL035C	0.05035752	0.09337738	0	0.0331771	0
YCL040W	0.17510338	0.5443327	0.58984893	0.64256626	0.441673944
YCL043C	0.20457833	0.16031443	0.10563908	0.20514929	0.070761124
YCL050C	0.33045551	0.1744834	0.03705753	0.04501843	0.100583527
YCL054W	1	0.86150684	0.94754589	0.83320687	0.935545763
YCL057W	0.31470575	0.1652987	0.04199831	0	0.024925103
YCR002C	0.85838557	0.67313058	0.69304333	0.82312946	0.739348958
YCR004C	0.73831194	0.87155336	0.92143297	1	0.955682956
YCR009C	0.93896639	0.97958103	0.93221344	0.89134249	0.919328373
YCR012W	0.10273251	0.17704078	0.09853541	0.13033229	0.169465471
YCR030C	0.85777337	0.88470449	0.87713351	0.86097468	0.921895924
YCR046C	0.94265321	0.98974295	0.97589915	0.81401528	1
YCR052W	1	0.7053465	0.93987542	0.8870685	0.5
YCR053W	0.11394502	0.05421619	0.02646195	0.01508436	0.046213793
YCR057C	1	0.87484263	0.94813408	0.95526605	0.869081708
YCR077C	1	0.80280173	0.78849059	0.62187434	0.532566227
YCR083W	0.02228207	0.18192039	0	0	0
YCR084C	0.22395589	0.09963356	0.04512387	0.05611725	0
YCR088W	0.05196887	0.08262694	0	0.01066828	0.000867577
YCR093W	0.95934805	0.71567373	0.90699318	0.94444024	0.854855547
YDL007W	0.95854853	0.90458569	0.82857946	0.87735497	0.91408629
YDL014W	0.99181221	0.9571691	0.94550237	0.80034269	0.832858223

YDL022W	0.19735122	0.21580722	0.10534509	0.11740158	0.127429335
YDL029W	0.75010506	0.73198004	0.60972401	0.5334037	0.703635899
YDL040C	0.98293775	0.86113864	0.94916908	0.82400729	0.731973456
YDL047W	0.79243451	0.37507693	0.4410093	0.39941642	0.261976873
YDL051W	0.25043919	0.15455428	0.08163515	0.2004278	0.100237263
YDL055C	0.67444072	0.65011548	0.38322391	0.48929237	0.596525993
YDL060W	1	1	0.91403503	0.85033106	0.772388038
YDL061C	1	0.98484937	0.83513426	0.66204653	0.553930932
YDL066W	0.11418949	0.0869523	0.2831867	0.50290144	0.602347932
YDL075W	0.81602309	0.82962221	0.64117796	0.65433821	0.533863785
YDL078C	0.68899278	0.73315737	0.81205831	0.62786364	0.800909196
YDL084W	0.17789248	0.15282238	0.10651558	0.09819677	0.196242637
YDL124W	0.03417948	0.03416949	0.02161318	0.01685577	0.071553102
YDL125C	0.06881086	0.061804	0.02293208	0.01597119	0.037348668
YDL126C	0.25841573	0.2663973	0.1851225	0.250449	0.255666064
YDL130W	0.80401826	0.7534291	0.79065713	0.69477008	0.651926846
YDL131W	0.49058335	0.2932917	0.38258417	0.30783328	0.354206407
YDL137W	0.86756079	0.96337021	0.68915621	0.77669573	0.774628804
YDL140C	0.25362606	0.44854088	0.35719917	0.15173814	0.438393381
YDL143W	0.97296518	0.80715599	0.86057419	0.86050485	0.931877644
YDL145C	0.85039996	0.65139804	0.81757171	0.63335504	0.811463376
YDL147W	0.85357793	0.55306581	0.47178742	0.58808586	0.789729888
YDL148C	1	0.90394794	0.99331705	0.99107456	0.986402884
YDL160C	0.94007768	0.8528802	0.85975532	0.75680305	0.762212847
YDL168W	0.07019067	0.13531166	0.03403163	0.03043677	0.071980962
YDL171C	0.53721489	0.44590333	0.36963155	0.59999096	0.660824131
YDL178W	0.39848781	0.08505431	0.20902405	0.04968683	0

YDL185W	0.49516748	0.36549651	0.22382673	0.25392982	0.364735742
YDL192W	0.91011713	0.75769798	0.54331334	0.59065823	0.515135097
YDL195W	0.6112483	0.24709874	0.15036454	0.36129034	0.629262385
YDL201W	0.14934676	0.29849457	0.03079227	0.01895463	0.023781516
YDL202W	1	0.94515921	1	0.90941011	0.912404715
YDL213C	0	0.14159648	0.44923706	0.61353891	0.305889192
YDL215C	0.91601148	0.7527834	0.6613183	0.59848905	0.817656655
YDL225W	1	0.18031302	0.74894808	0.76933634	0.749827299
YDL229W	0.4013291	0.34900802	0.35975932	0.4135175	0.476398044
YDR001C	0.56100717	0.44322921	0.56745005	0.44978562	0.46132622
YDR002W	0.1053619	0.08241233	0.00327535	0.01099617	0.056937046
YDR019C	0.14644287	0.1096071	0.01905897	0.11749245	0.388389792
YDR021W	1	1	0.9740467	0.8340355	1
YDR023W	0.07357134	0.07203557	0.08332178	0.1762542	0.23066703
YDR032C	0.36377512	0.32023726	0.2531347	0.30057073	0.637792261
YDR035W	0.21841803	0.1307504	0.08690276	0.17741194	0.248165418
YDR037W	0.3366452	0.27229704	0.18471177	0.17190169	0.11760513
YDR050C	0.13736816	0.16800909	0.0934464	0.06023959	0.066396534
YDR060W	1	0.97139927	0.97663692	0.82449923	0.93590929
YDR064W	0.87777012	0.91789368	0.90058306	0.70618291	0.691935869
YDR071C	0.23653237	0.17378711	0.09208203	0.11382641	0.142907609
YDR074W	0.51746981	0.30253958	0.30802394	0.11848194	0.068596735
YDR087C	0.92724854	0.83889457	0.98465776	0.94128896	0.837029463
YDR091C	0.92274796	0.7446375	0.86398122	0.78927142	0.706049435
YDR098C	0.03322066	0.08597323	0.07587628	0.13839698	0.063371903
YDR099W	0.16123153	0.14928637	0.05927972	0.12126387	0.134012578
YDR101C	0.94630542	0.81072415	0.84683178	0.7693049	0.677201453

YDR117C	1	0.91923175	0.96046584	1	1
YDR120C	0.90023593	0.22463498	1	0.96217778	0.860231014
YDR127W	0.19149904	0.39122087	0.19894631	0.33136735	0.643488492
YDR129C	0.49746768	0.28063481	0.12324965	0.11614585	0.169634167
YDR141C	0.79226424	0.9691648	0.98268675	0.96882432	0.923237753
YDR148C	0.82898971	0.80614534	0.92673909	0.77957664	0.832176053
YDR150W	0.92881847	0.63656421	1	0.90993569	0.792375876
YDR155C	0.07742462	0.13566693	0.04091022	0.07167524	0.060378874
YDR158W	0.28448266	0.13182166	0.05790065	0.08953111	0.168543282
YDR164C	0.93631163	1	0.99526913	0.86185913	0.963792499
YDR165W	0.16205947	0.23560956	0	0.06050003	0
YDR166C	1	0.85735234	0.87432867	0.91538495	0.914511122
YDR168W	0.17217373	0.0211452	0.07115828	0.0209629	0
YDR170C	0.94519307	0.5663327	0.65514803	0.75588718	0.889049151
YDR171W	0.92101602	0.29186242	0.78286773	0.71607908	0.738330096
YDR172W	0.90900152	0.80245392	0.61642873	0.85820472	0.735167716
YDR174W	0.84935983	0.82833811	0.90632929	0.75861254	0.798839478
YDR175C	0.90042574	0.93062609	0.98954108	0.67566544	0.858312985
YDR176W	1	0.90488266	0.83791016	1	0.869334085
YDR188W	0.9704484	0.91162597	0.76450628	0.80498543	0.894066157
YDR190C	0.87118025	0.87529909	0.62055268	0.69856935	0.732276441
YDR194C	1	0.96484565	1	0.93997535	0.813140335
YDR211W	1	0.77431705	0.86840503	0.72896557	0.965721558
YDR212W	0.88988908	0.80814997	0.76351544	0.78156593	0.822873237
YDR214W	0.12183568	0.0425831	0.01615496	0.14585145	0.2048823
YDR226W	0.04132121	0.04550139	0.01648787	0.06906812	0.051955435
YDR233C	0.91588712	0.9893715	0.97918336	0.93843027	0.955473035

YDR234W	0.87916969	0.23161585	0.17377074	0.29520053	0.439817836
YDR238C	0.92043655	0.83897781	0.83688223	0.6875045	0.910093345
YDR258C	0.26210255	0.10905208	0.10454682	0	0
YDR289C	0.8226575	0.79275365	0.88577558	0.84041964	1
YDR293C	0.81962087	0.84123906	0.80580959	0.61979508	0.601059725
YDR296W	1	0.9397918	0.9364142	0.85241886	1
YDR298C	0.66024808	0.48302196	0.48179478	0.49608792	0.530088125
YDR301W	1	1	1	1	1
YDR303C	0.95350747	0.91850133	0.9720246	0.93266071	0.449592681
YDR304C	0	0	0	0	0
YDR322W	0.88771584	0.96482112	0.98737881	0.92988975	0.479028572
YDR324C	1	0.93910048	0.96489109	0.88853366	0.585435147
YDR341C	0.32932156	0.14460352	0.09974062	0.16665699	0.22781646
YDR353W	0.10025612	0.01820677	0.04551427	0.05324741	0.098363703
YDR368W	0.04668893	0.17076223	0.00179675	0	0.027115393
YDR381W	0.85721386	0.9011443	0.87443307	0.69254609	0.631350439
YDR382W	0.8805624	0.82147977	0.83762119	0.75970415	0.698902588
YDR388W	0.94342433	0.99186093	0.98818326	0.86439662	0.903317572
YDR394W	0.89256074	0.88931037	0.92847438	0.78318081	0.877943994
YDR395W	0.96536642	0.87001664	0.96537905	0.87509738	0.934106389
YDR399W	0.03194138	0.03042963	0	0.07879671	0.012097346
YDR408C	0	0.04557037	0	0	0.116414139
YDR427W	0.73204468	0.53027428	0.49837611	0.67264182	0.807005798
YDR429C	0.91783773	0.52151088	0.79168394	0.72902398	0.774737438
YDR430C	0.24867992	0.22491806	0.10062956	0.03223394	0.127698955
YDR432W	0.26741016	0.32021961	0.3762028	0.39684415	0.414625808
YDR449C	1	0.97256784	0.98755953	0.93655694	0.991099311

YDR454C	0.03719409	0.01504838	0.02366859	0.0139615	0.008849708
YDR457W	0.93603026	0.65811802	0.51512466	0.78948694	0.84810566
YDR472W	1	0.85263786	0.74789764	1	0.891871905
YDR483W	0.83043716	1	0.96201184	0.98448063	1
YDR496C	0.99950044	0.81471878	0.93319341	0.7718576	0.875118882
YDR502C	0.73517057	0.52161478	0.10750659	0.36494376	0.333814662
YDR513W	0.07174692	0.11741435	0.04320037	0.17092781	0.040441905
YDR516C	0.19454234	0.17740934	0.0860795	0.06716275	0.111172521
YDR533C	0.08551873	0.09119116	0.01059693	0.02240844	0.090301429
YEL002C	0.92819276	0.94022831	0.97762425	0.96389854	0.973508104
YEL011W	0.03611301	0.0555495	0.00403921	0.04701179	1
YEL013W	1	0.94962021	0.92461192	0.83877416	1
YEL021W	0.15661473	0.01059603	0.00657877	0.00811299	0.194268976
YEL024W	1	0.97605594	0.74285272	1	0.721672524
YEL037C	0.17186203	0.03345219	0.05395541	0.08536942	0.078405232
YEL038W	0	0.0439335	0	0	0.050331694
YEL047C	0.01892637	0.05969651	0.00323468	0.02599291	0.011318368
YEL051W	1	0.75927878	0.84993579	0.48706534	0.655078033
YEL055C	0.96055455	0.90890064	0.98012555	0.94764832	0.909015865
YEL060C	0.19302402	0.26772359	0.16924251	0.26730339	0.776333298
YER003C	0.12448593	0.03451813	0.04044054	0.02529748	0.022555973
YER009W	0.23199189	0.12570648	0.0432565	0.06617076	0.077361893
YER012W	0.16435658	0.07938664	0.19254246	0.16200735	0.199204405
YER021W	0.87463106	0.56041642	0.65987827	0.69877264	0.773525113
YER023W	0.73305784	0.49529783	0.35787366	0.07417312	0.168101912
YER024W	0.64719633	0.50448272	0.51927795	0.16956756	0.5
YER025W	0.68167323	0.71920465	0.68817427	0.66281674	0.533728393

YER036C	0.82012825	0.71398298	0.72592393	0.81423526	0.697474973
YER042W	0.03835004	0.10347811	0.01044201	0.05518645	0.080800854
YER043C	0.49452442	0.404916	0.25123288	0.29956974	0.373561916
YER048W-A	0.80767583	0.83163009	0.85875622	0.76412193	0.734475539
YER052C	0.77938938	0.31414603	0.23113188	0.10617977	0.182817986
YER055C	0.52462209	0.17483514	0.12348159	0.08522	0.15149546
YER057C	0.22595196	0.15909574	0.04056443	0.06513321	0.263239745
YER069W	0.82366785	0.52347339	0.07107368	0.28284849	0.101656556
YER080W	0.90049555	0.60119511	0.53445337	0.56834664	0.888944368
YER081W	0.22200215	0.19763821	0.03397016	0.06065449	0.115626903
YER086W	0.86436151	0.77906403	0.78513756	0.80481005	0.922232796
YER090W	0.22954098	0.27397867	0.02271812	0.09107487	0.223190847
YER091C	0.04786044	0.08420738	0.03718064	0.13168993	0.078402021
YER094C	0.23688075	0	0.12394486	0.06399565	0.090919123
YER110C	0.80272808	0.47177249	0.42444735	0.32957446	0.656919099
YER112W	1	0.78273337	0.77782142	0.50748061	0.786492347
YER114C	0.72959457	0.97861893	0.84929916	1	1
YER126C	1	1	0.98990518	0.9718557	0.903558794
YER133W	0.45996925	0.41651618	0.51096532	0.52254337	0.769981508
YER136W	0.05554016	0.08194154	0.05183589	0.17467829	0.075156686
YER143W	0.19379792	0.12739132	0.02812111	0.26139892	0.16890366
YER151C	0.83941224	0.93992629	0.96042772	0.89992418	0.863527835
YER155C	0.97928441	0.75212812	0.94954524	0.92459016	0.592646499
YER165W	0.19073412	0.11930369	0.16563481	0.47099074	0.525261083
YER166W	1	0.92123106	1	1	1
YER178W	0.86274089	0.76516635	0.90617988	0.83115569	0.920704987
YFL002C	1	1	0.93491785	0.98146954	0.981116003

YFL005W	0.88315983	0.87562521	0.8181896	0.74203093	0.803794004
YFL014W	0.57181345	0.23673884	0.03996729	0	0.112083089
YFL018C	0.36676863	0.32094546	0.36831713	0.49410907	0.714319502
YFL022C	0.28680614	0.31432292	0.11508307	0.20653818	0.176278389
YFL037W	0.93460992	0.83898999	0.88527979	0.85348622	0.872252725
YFL038C	1	0.78611448	0.84691687	0.72175938	0.817417112
YFL039C	0.51691162	0.38321529	0.28150934	0.29414885	0.442883725
YFL041W	1	0.8953868	0.92567094	0.9082047	1
YFL045C	0.1810495	0.16409607	0.09487459	0.13757816	0.092530496
YFL048C	1	0.91471814	1	1	1
YFR001W	1	0.60979459	0.91817757	0.71332597	0.566927551
YFR004W	0.61322648	0.37344904	0.58335443	0.70143484	0.671638775
YFR006W	0.00586243	0.04719329	0.04315828	0.01639195	0.149417653
YFR009W	0.66421664	0.76542015	0.58069993	0.89585432	0.819259314
YFR010W	0.18869648	0.33497673	0.20555712	0.13842678	0.39054436
YFR015C	0.81159722	0.73414134	0.37603019	0.268485	1
YFR024C-A	0.86047575	0.5584656	0.97362147	0.89522724	0.845231751
YFR037C	0.90824802	0.90966904	0.93977252	0.84575657	0.990003748
YFR044C	0.21096331	0.14974689	0.11493834	0.03083972	0.099533391
YFR052W	0.73657326	0.56027784	0.60287221	0.546367	0.641459397
YFR053C	0.07768066	0.11381283	0.04415398	0.05764761	0.003523252
YGL008C	0.9969616	0.85750428	0.98361776	0.96401016	0.96722786
YGL009C	0.42413798	0.1315075	0.02894696	0.0129459	0
YGL011C	0.16509177	0.17579166	0.05767127	0.10315688	0.053366724
YGL014W	0.90019927	0.93679631	1	0.75341024	0.856987761
YGL019W	0.89080304	0.76297795	0.96555727	0.67962129	0.788857354
YGL026C	0.18529452	0.20929777	0.11198312	0.09804623	0.158525633

YGL030W	0.68820776	0.78759767	0.75129883	0.63745541	0.621900935
YGL031C	0.94617094	0.86425567	0.89796724	0.80303112	0.750706097
YGL037C	0.11146511	0.08920809	0.19873911	0.29835698	0.431912242
YGL040C	0.05243541	0.12483467	0.03245943	0.04801791	0.030077529
YGL048C	0.86126618	0.8236376	0.8701392	0.80248958	0.778492061
YGL054C	1	1	1	0.93377533	0.939457331
YGL056C	0.21727595	0.1840695	0.12416107	0.12733071	0
YGL064C	0.97595245	0.9458373	1	0.94962217	1
YGL068W	0.87945137	0.80268262	0.92139181	0.80470147	0.742939871
YGL076C	0.90149826	0.91589148	0.83534335	0.70911066	0.642287112
YGL097W	0.67678022	0.78976274	0.77428182	0.28465661	0.435653884
YGL099W	1	0.84003068	0.91236794	0.92952026	0.900603171
YGL103W	0.8051291	0.89908629	0.84151667	0.61773995	0.648216989
YGL105W	0.15162451	0.17567692	0.11956038	0.16188757	0.120381907
YGL111W	1	1	0.94883489	0.95646213	0.830758718
YGL112C	1	0.93114766	0.97044724	0.94086828	0.990027777
YGL120C	0.97513971	0.90962172	0.89442898	0.83981956	0.780987172
YGL123W	0.8994491	0.93513761	0.91113209	0.74138168	0.71548985
YGL129C	1	0.97297716	0.92000944	0.87110076	0.754767997
YGL137W	0.81341567	0.52872753	0.69478571	0.53710238	0.808163068
YGL147C	0.89654411	0.91338001	0.86672689	0.67771636	0.662701637
YGL148W	0.0774867	0.08673119	0.01739877	0.11369881	0.147035598
YGL150C	0.98017324	0.97954601	0.87929852	0.95922473	0.827741288
YGL151W	0.97941337	0.96623876	0.97403002	0.98265041	1
YGL156W	0.37187911	0.51558995	0.52164972	0.43063555	0.287654498
YGL167C	0.97943792	0.98425314	1	0.95772623	1
YGL173C	0.75985172	0.84248437	0.72793312	0.55712321	0.699732657

YGL195W	0.98415049	0.85062997	0.85754949	0.83734268	0.907742762
YGL200C	1	0.91559627	0.98460528	0.93594125	0.987424506
YGL202W	0.08120356	0.11664231	0.01798736	0.10311529	0.094980377
YGL207W	0.14801139	0.24414952	0.14383261	0.16124973	0.149888434
YGL210W	0.87733717	0.93250573	0.87813736	0.92224731	0.863462313
YGL221C	0.18234393	0.16173214	0.02948283	0	0.006405233
YGL234W	0.46964401	0.26996021	0.22734642	0.17964419	0.330959256
YGL245W	0.13540148	0.23699055	0.12845533	0.18792736	0.13958704
YGL246C	1	0.97044952	0.87154172	0.66516475	0.541899822
YGL252C	0.8738376	0.94534418	0.7378685	0.64406174	0.678184139
YGL253W	0.14072684	0.10108542	0.08176612	0.06801522	0.079814867
YGR020C	0.34545431	0.19570497	0.12693812	0.10513106	0.080692937
YGR043C	0.24104942	0.28807244	0.22972308	0.19438444	0.5
YGR054W	0.72222492	0.4993957	0.76621249	0.69334522	0.648478037
YGR061C	0.10418961	0.07751655	0.07581417	0.13601918	0.110383395
YGR086C	0.82220256	0.59348402	0.44155234	0.30614554	0.333614494
YGR087C	0.21355605	0.19845717	0.07745723	0.07877453	0.270801556
YGR090W	0.98745014	0.96466435	0.93708187	0.88329875	0.833748972
YGR094W	0.12297119	0.0695118	0.03375482	0.04661051	0.087596921
YGR103W	0.91183138	0.81851214	0.93971654	0.81486575	0.756827157
YGR124W	0.09447651	0.08249714	0.00335825	0.01752936	0.036855319
YGR128C	1	0.94209439	0.95812205	0.9515761	0.880977401
YGR130C	0.84060723	0.74411439	0.40366047	0.22876128	0.904836667
YGR132C	1	1	0.96019376	1	1
YGR135W	0.38064259	0.14965397	0.08080971	0.14512951	0
YGR148C	0.97142606	0.93027335	0.86820325	0.94828672	0.786939693
YGR155W	0.18128588	0.22915906	0.11044283	0.16876973	0.219102797

YGR162W	0.76425091	0.83454224	0.736871	0.66187376	0.689738024
YGR180C	0.45202507	0.17178226	0.1169714	0.09022499	0.14540497
YGR185C	0.73572337	0.59848027	0.66110692	0.62240259	0.555947415
YGR192C	0.42054075	0.33604383	0.30317701	0.38515884	0.426413245
YGR193C	1	0.79242407	0.99347482	0.98424938	1
YGR198W	0.95767683	1	1	1	0.5
YGR200C	0	0.09150655	0.50205374	0.55400278	0.534952057
YGR204W	0.84904252	0.62327376	0.70368095	0.76855777	0.75075317
YGR205W	0.43220316	0.10007369	0	0.01753988	0.323104792
YGR209C	0.21172224	0.14419908	0.06469079	0.12047481	0.113851143
YGR210C	0.96717185	0.96704052	0.87003474	0.70775589	0.600036442
YGR211W	0.13176411	0.14911261	0.07773516	0.12821117	0.168886904
YGR218W	0.9266752	0.78531827	0.83199634	0.58123448	0.902530721
YGR240C	0.38173909	0.4110111	0.39886621	0.50454143	0.445249063
YGR253C	0.29056533	0.08693774	0.11978525	0.15990758	0.098155687
YGR254W	0.10071642	0.13237046	0.07527378	0.11153571	0.130937156
YGR256W	0.293991	0.25541648	0.22575447	0.23605569	0.563255165
YGR264C	0.19961221	0.39977877	0.15681924	0.24354788	0.16415184
YGR267C	0.83170443	0.76066801	0.74217693	0.59224468	0.708215017
YGR282C	0.30250303	0.37025114	0.2838035	0.36600945	0.592184141
YGR285C	0.75189542	0.54588777	0.68426975	0.74157086	0.682605554
YHL011C	0.79446183	0.67758972	0.74909923	0.7746287	0.724379212
YHL015W	0.8428008	0.80663729	0.78641376	0.68591115	0.683525412
YHL021C	0.05986221	0.09048613	0.04640408	0	0
YHL033C	0.88314105	0.90736027	0.87144869	0.74409495	0.671772883
YHL034C	0.11110246	0.18476178	0.21687222	0.39105355	0.301938701
YHR007C	0.8269098	1	1	1	0.997581163

YHR008C	0.22792277	0.28263061	0.24822945	0.17540506	0.203310501
YHR012W	1	0.62369263	0.81393345	0.52955055	0.810212696
YHR013C	0.96131195	0.94071565	0.88298956	0.74539537	0.596645444
YHR018C	0.08292483	0.09002903	0	0.01345973	0.023736179
YHR019C	0.22741997	0.20219459	0.22473202	0.29695476	0.294838334
YHR020W	0.42221887	0.29644959	0.2740553	0.31757461	0.24189162
YHR025W	0.95265256	0.24328685	0.36837332	0.34562662	0.485195765
YHR027C	0.92421703	0.72958253	0.84124447	0.71084161	0.80239664
YHR037W	0.19165026	0.15384883	0.04496195	0.03023791	0.124990184
YHR051W	0.71582901	0.70151533	0.75435493	1	0.511079381
YHR052W	0.95495249	0.84919032	0.84640946	0.85713226	0.777231768
YHR062C	0.89826404	1	0.97084242	0.64117284	0.925655922
YHR064C	0.71025466	0.60948424	0.67907043	0.64199575	0.589543972
YHR068W	0.03089119	0.02389331	0.01931542	0.02052648	0.039313264
YHR087W	0	0.03783822	0.02361586	0	0.12031914
YHR088W	1	0.99331029	0.99756729	0.97528423	0.944772365
YHR089C	0.91948466	0.91241182	0.81600051	0.7312682	0.655627583
YHR097C	0.88019504	0.85335489	0.80710353	0.84372354	0.648071591
YHR099W	0.97509033	0.92532342	0.85463431	0.94815556	0.97550402
YHR104W	0.02172104	0.03102225	0.00067487	0.03593642	0.055317122
YHR107C	0.65089056	0.56554882	0.79498375	0.74121737	0.778097748
YHR113W	0.24450488	0.25505777	0.13597432	0.03219613	0.244142802
YHR121W	0.33009072	0.48839638	0.85890811	0.69985327	0.732931866
YHR127W	1	0.95612255	0.93909463	0.90009579	0.923915774
YHR128W	0.05094882	0.15420244	0.01482609	0.01129098	0.030928674
YHR139C	0.1123721	0.1199241	0.06050086	0.04147645	0
YHR163W	0	0	0.10758097	0.08237425	0.049216666

YHR169W	1	1	1	0.92710458	0.956995332
YHR170W	0.72646219	0.67064282	0.79456292	0.71716445	0.715581653
YHR174W	0.11869591	0.15344844	0.08203108	0.13379712	0.148163901
YHR183W	0.22822097	0.25138376	0.22040536	0.2171598	0.292288028
YHR193C	0.41127326	0.32517803	0.48445232	0.60985423	0.525633308
YHR197W	1	0.76531247	0.95702639	0.91264353	0.818841614
YHR200W	0.44083563	0.41153012	0.30601208	0.47122252	0.373106844
YHR208W	0.03224051	0.28299667	0.02802162	0.07316597	0.037643898
YIL005W	0.93399061	1	1	1	0.988175257
YIL010W	0.71583446	0.7230009	0.58710539	0.83210134	0.559339012
YIL022W	1	0.7981764	0.95741998	0.86383984	0.825477862
YIL033C	0.21334571	0.16829706	0.10662644	0.12910012	0.103961485
YIL035C	0.95380071	0.88347553	0.99090795	0.86384109	0.947838245
YIL041W	0.79423742	0.56324541	0.52273953	0.61003108	0.661912715
YIL051C	0.08932405	0.0540268	0.01311573	0.07702875	0.100928297
YIL053W	0.69328458	0.30452176	0.12480234	0.19763475	0.244167115
YIL055C	0.51405301	0.6104507	0.69187555	0.74455737	0.39931842
YIL062C	0.8017351	0	0.29768225	0.27872348	0.283673852
YIL070C	0.28216347	0.15027317	0.11580672	0.02761762	0.21890316
YIL074C	1	0.09343777	0.07585381	0.04996182	0
YIL075C	0.87245141	0.82503629	0.87260762	0.80968198	0.855035431
YIL076W	0.94960372	0.82548892	0.76442773	0.50021817	0.816611679
YIL078W	0.55901431	0.79228855	0.4558637	0.4354943	0.494247163
YIL083C	0.13978704	0.06697545	0.00955088	0.05356102	0
YIL091C	0.81721159	0.50131614	0.83718287	0.76946497	0.717478737
YIL094C	0.32266651	0.27347481	0.15079935	0.06550666	0.365633843
YIL105C	1	0.92220166	1	1	0.82338399

YIL109C	0.26975832	0.2446299	0.21537892	0.50210515	0.482910499
YIL116W	0.24955384	0.04236213	0.09123284	0.06863507	0.074491548
YIL124W	0.90873671	0.94649006	0.94183128	1	1
YIL125W	0.73478129	0.71204631	0.84756247	0.78712466	0.746020009
YIL126W	0.91726843	0.79895405	0.94027059	0.96359002	0.943050175
YIL128W	0.95817715	0.94052221	0.94404434	0.94129691	0.943651679
YIL133C	0.90427693	0.95298036	0.88854725	0.72552639	0.65550221
YIL137C	0.79440453	0.58670688	0.933772	0.72329304	0.92323224
YIL142W	0.89058378	0.7861441	0.62762167	0.74627246	0.741879674
YIL162W	0.12944402	0.19231895	0.08401692	0.01518126	0.182749149
YIR037W	0.03052074	0.10794487	0.01605721	0.01319469	0.031713173
YJL002C	1	1	1	1	1
YJL005W	0.91688465	0.86328747	0.94322016	0.82821343	0.512924381
YJL008C	0.93393756	0.77061632	0.69086627	0.74761996	0.778374794
YJL010C	0.86937064	1	0.72926309	0.76082444	0.728370567
YJL014W	0.83907921	0.71183265	0.63022456	0.67021908	0.778113408
YJL026W	0.58462312	0.37043608	0.20904099	0.18434633	0.320704325
YJL033W	0.87160581	0.98995657	0.98007794	0.79581923	0.802380593
YJL034W	0.63496725	0.41023838	0.29001705	0.58277912	0.636650992
YJL050W	1	0.80672705	0.91184593	0.72953544	0.662855797
YJL052W	0.39881648	0.24366445	0.21387067	0.225732	0.169044863
YJL080C	0.41395639	0.4350475	0.41698541	0.49967434	0.549546998
YJL081C	0.65950827	0.60537347	0.62213598	0.63038852	0.761088287
YJL109C	0.99783407	0.93898194	0.97536221	0.97476683	0.974836106
YJL111W	0.90938566	0.84868306	0.59468771	0.64606674	0.680015879
YJL115W	0	0.06184205	0	0	0.033506969
YJL123C	0.68672432	0.2413705	0.25504755	0.2386467	0.225088171

YJL124C	0.75451164	0.24897952	0.49507086	0.4087904	1
YJL130C	0.8492202	0.82041993	0.86518766	0.91770979	0.630322736
YJL136C	0.72755986	0.41708425	0.2819009	0.30578975	0.308734757
YJL153C	0.12616774	0.17643098	0.04408329	0.03719149	0.03908244
YJL164C	0.18609726	0.11369142	0.06550256	0	0.152950896
YJL167W	0.27967415	0.0806979	0.11303767	0.06825831	0.085935795
YJL172W	0.11162434	0.39544498	0.50827618	0.53449646	0.715644376
YJL177W	0.89559826	0.87630828	0.83733047	0.74188403	0.720200654
YJL178C	1	0.74339782	1	1	0.660640702
YJL200C	0.17990531	0.04362079	0.01309088	0.05189622	0.091451078
YJR007W	0.53598116	0.47957207	0.56782255	0.49489378	0.472482531
YJR009C	0.67275375	0.49640833	0.42600305	0.30045679	0.479442845
YJR016C	0.0731829	0.12647116	0.06883838	0.22706652	0.234692516
YJR041C	1	1	0.99282883	0.9552517	1
YJR045C	0.42081308	0.32141366	0.18109186	0.18045355	0.253708832
YJR048W	0.46706727	0.28974343	0.44909687	0.50906123	0.457581094
YJR064W	0.74866264	0.40217899	0.42694027	0.70375696	0.638126313
YJR065C	0.89749066	0.73888141	0.6555098	0.58235562	0.749212392
YJR068W	1	0.99528216	0.96268466	0.91726379	0.86925994
YJR070C	0.42364323	0.09127781	0.06044041	0.14938504	0.167947942
YJR076C	0.41780241	0.17989301	0.70438684	0.68956539	0.54512357
YJR077C	1	0.97629663	0.97596645	0.93633289	0.992516234
YJR103W	0.20796392	0.29553888	0.07826642	0.16725104	0.5
YJR104C	0.07287692	0.1096769	0.03493985	0.06180889	0.009768533
YJR105W	0.04454573	0.1625398	0.02348328	0.01049487	0.023329037
YJR109C	0.17875862	0.09441273	0.05309901	0.03351255	0.047513706
YJR121W	0.69939103	0.64840809	0.56056953	0.45875406	0.617131885

YJR123W	0.83387073	0.83298441	0.70016145	0.6259957	0.568901317
YJR132W	0.91306297	0.86975971	0.94538143	0.95670312	0.847789515
YJR139C	0.20052567	0.26804889	0.0831413	0.04124506	0.149713048
YJR148W	0.04751172	0.1552058	0.00315892	0.06491059	0.038649146
YKL007W	0.5272421	0.12730223	0.05650461	0.08052281	0.273344355
YKL009W	0.61977093	0.73294261	0.76439656	0.80014242	0.709061809
YKL013C	0.60178459	0.34015338	0.32647282	0.13512445	0.462629778
YKL018W	0.88198216	0.89546061	0.90729016	0.83540848	1
YKL019W	1	0.07864768	0	0	0.350881445
YKL021C	0.55554928	0.8376037	0.856479	0.75318893	0.81899881
YKL035W	0.27011715	0.50057441	0.52616519	0.5729489	0.503884905
YKL039W	0.7516044	1	1	1	0.936435077
YKL050C	0.91799421	0.80016396	0.65053014	0.56795659	0
YKL056C	0.12481802	0.09961924	0.05538706	0.16157034	0.092142166
YKL060C	0.28449571	0.14222823	0.07716644	0.133417	0.118180314
YKL067W	0.10227475	0.14032399	0.08332384	0.09781658	0.096246055
YKL077W	1	0.8125498	0.85160712	1	1
YKL080W	0.4662419	0.19746659	0.1919871	0.16759421	0.251365188
YKL081W	0.34413786	0.27630485	0.36884997	0.43304424	0.328045077
YKL085W	0.09055397	0.10843905	0.093473	0.0747892	0.109908877
YKL096W	0.26896941	0.17734495	0.15113737	0.30092954	0.569279597
YKL103C	0.26655735	0.29402896	0.1848452	0.06825463	0.053164315
YKL104C	0.90874973	0.84739052	0.70483235	0.70613153	0.814602082
YKL106W	1	0.91378078	0.96456535	0.72080515	0.944992827
YKL117W	0.0606083	0	0	0.02289134	0.038409204
YKL135C	1	0.94296711	0.91681863	0.68071492	0.72284487
YKL142W	0.09919085	0.11086786	0.02960411	0.02855109	0.009943672

YKL145W	0.88337489	0.8329455	0.8714849	0.74073993	0.90116787
YKL148C	0.54902678	0.54860296	0.53559007	0.45925541	0.846949394
YKL150W	0.28382832	0.3564269	0.44540581	0.26453773	0.14296343
YKL151C	0.38781981	0.4309567	0.35708307	0.266126	0
YKL152C	0.23335206	0.39404911	0.18255211	0.2147204	0.26728246
YKL157W	0.34282639	0.17661277	0.07346184	0.06390155	0.340911802
YKL180W	0.90778895	0.88910944	0.83271489	0.68856573	0.594289311
YKL182W	0.70028698	0.50981403	0.7458278	0.77191426	0.622515858
YKL193C	0.16254054	0.0753782	0.12369932	0	0
YKL203C	1	1	1	1	0.985153682
YKL210W	0.05639199	0.05881386	0.01475249	0.03443695	0.037419325
YKL212W	1	0.86276837	0.88091296	1	1
YKL213C	0.06598164	0	0.0187392	0.23843289	0.5
YKR001C	0.8553634	0.71893994	0.93358898	0.87973863	0.914065436
YKR008W	0.80110076	0.73926781	0.90758611	0.94892381	0.94067277
YKR014C	0.86037235	0.7847944	0.58838429	0.92482839	0.647251418
YKR026C	1	1	0.76899308	0.97382019	0.96945077
YKR043C	0.11253367	0.05690702	0.06636846	0	0.024595746
YKR046C	0.9455362	0.79038694	0.83348539	0.79813255	1
YKR048C	0.46855319	0.12211673	0.06496136	0.12923435	0.038015186
YKR066C	0	0.0883803	0.01325611	0.07055667	0
YKR074W	0.02815182	0	0	0	0
YKR080W	0.01022047	0.12674089	0.05136734	0.02903772	0.015970998
YKR081C	0.61890631	0.77174411	0.74969974	0.62493603	0.888230311
YLL001W	0.89478644	0.65716525	0.4941108	0.32797511	0.587943361
YLL018C	0.31386988	0.33981951	0.27933244	0.31958016	0.381769105
YLL024C	0.41420913	0.2737039	0.2351733	0.26931095	0.323426137

YLL026W	0.22059195	0.17495096	0.09173962	0.19031783	0.106233014
YLL029W	0.66148499	0.86355334	0.83372534	0.86282935	1
YLL036C	0.93782793	0.92663263	0.95774543	1	0.882190941
YLL045C	0.8479482	0.91020195	0.83970818	0.61479932	0.61663282
YLL050C	0.07079027	0.04061673	0.01835308	0.06435828	0.053189022
YLR002C	0.92319347	1	1	0.94898061	0.969983863
YLR009W	1	0.91405231	0.9867352	0.97927647	0.537236168
YLR017W	1	0	0.34663291	0.6478732	0.692333452
YLR027C	0.19766045	0.14568888	0.01081276	0.03037726	0.088342794
YLR028C	0.08946934	0.24827193	0.0115152	0.03797187	0.081002497
YLR029C	0.99945666	0.99802315	0.9701672	0.8162103	0.77716269
YLR033W	1	1	1	0.88510051	1
YLR043C	0.12697438	0.09766847	0.0335695	0.05519426	0.184213273
YLR044C	0.16206081	0.16561855	0.08648671	0.12999091	0.129588312
YLR048W	0.71826782	0.57629662	0.48023077	0.39572239	0.479875052
YLR058C	0.33184846	0.23943207	0.33998769	0.50595618	0.467387465
YLR060W	0.0960185	0.17590252	0.11199415	0.16744666	0.148231447
YLR061W	0.60668142	0.70535591	0.66885239	0.57594423	0.555427574
YLR069C	0.09989211	0.39410494	0	0.01845958	0
YLR075W	0.89702485	0.92625747	0.88497842	0.7476433	0.707733232
YLR109W	0.04395164	0.10446999	0.02826966	0.04714257	0.051888813
YLR150W	0.72493736	0.76402488	0.62965642	0.71188735	0.553467372
YLR153C	0.21820156	0.35320848	0.34959759	0.55725377	0.453581351
YLR163C	0.74189284	0.48966696	0.12443622	0.03960768	0.274042591
YLR167W	0.51950414	0.63086102	0.46034544	0.46433327	0.487682402
YLR172C	0.01382301	0.09211642	0.01789858	0	0.041024494
YLR174W	0.36494043	0.22475892	0.14115704	0.14786805	0.366700683

YLR175W	0.81008541	0.89165766	0.92924498	0.72549393	0.699647467
YLR178C	0.02833452	0.07707589	0.03054313	0.05283234	0
YLR180W	0.67872998	0.53369507	0.34007174	0.34087416	0.28005891
YLR195C	0.07597859	0.10615867	0.01978796	0.17303006	0.112639431
YLR196W	0.83303017	0.83901407	0.62434672	0.69161531	0.397628737
YLR197W	0.95189323	0.90697327	0.90450896	0.84675417	0.85059726
YLR208W	0.52416742	0.37434111	0.3068786	0.61552349	0.695920267
YLR209C	0.17269253	0.01461757	0.02077222	0	0.32606075
YLR216C	0.16402641	0.15871918	0.01769997	0.27514559	0.399368658
YLR222C	1	0.70994162	0.9514983	0.97920756	0.973559636
YLR231C	0.06275157	0.11443303	0.00871588	0	0.638370446
YLR244C	0.94496939	0.82430525	0.93850244	0.79986254	0.827923017
YLR249W	0.64889387	0.55135606	0.42507619	0.35818618	0.36360626
YLR250W	1	0.95487308	0.93431982	0.96409703	1
YLR259C	0.4194227	0.43950729	0.22494681	0.27954154	0.241155111
YLR262C	1	0.90593751	1	1	1
YLR270W	0.03900675	0.09628313	0.03004756	0.03480971	0.013597464
YLR290C	1	0.92291419	1	1	1
YLR291C	1	1	1	0.98951293	0.944411393
YLR303W	0.21667322	0.06305379	0.03208735	0.0777209	0.122757078
YLR304C	0.1030053	0.1057278	0.02520591	0.0696824	0.094275134
YLR312W-A	0.87869928	0.89998416	0.88493461	0.70219856	0.890225634
YLR321C	1	1	1	0.81505517	0.919353003
YLR325C	0.95979233	0.8468581	0.9093774	0.74500491	0.659350618
YLR330W	0.78596829	0.84373902	0.86391535	0.87380131	0.836647492
YLR340W	0.71954259	0.74645057	0.67418692	0.73383943	0.668001494
YLR342W	1	0.78774585	0.98678446	0.99739514	0.947833004

YLR347C	0.90163321	0.73839457	0.82043444	0.57022327	0.852349647
YLR354C	0.03947297	0.08775494	0.02169248	0.06067554	0.076477173
YLR355C	0.57758512	0.41665999	0.2711769	0.29402948	0.493140053
YLR357W	1	0.79369322	0.80066969	0.90460336	1
YLR359W	0.0892455	0.14691052	0.03434689	0.10549435	0.096368847
YLR370C	0.8478216	0.76234663	0.25522015	0.42740679	0.558639214
YLR378C	0.99058195	0.86992182	1	0.99302804	1
YLR384C	0.92250196	0.83629415	0.80570766	0.86848101	0.82399656
YLR388W	1	0.9677599	0.84994169	0.61196083	0.630104826
YLR398C	0.9653969	0.91126713	0.88703173	0.93642303	0.922543461
YLR411W	0.99690975	1	1	0.96582656	0.973939757
YLR420W	0.0734672	0.03862035	0.01260339	0	0
YLR421C	0.80649057	0.96536351	0.72950131	0.7078211	0.369088398
YLR429W	0	0	0.02745344	0	0.090838678
YLR432W	0.79172499	0.71414982	0.72236695	0.69982904	0.616247739
YLR438W	0.09367896	0.11595472	0.04174338	0.07761527	0.145868851
YLR439W	1	0.97248654	0.87339552	1	0.735937489
YLR441C	0.97836432	0.99009015	0.89218222	0.75254365	0.76496341
YLR447C	0.9853472	0.86350064	0.92775125	0.88422788	0.964143478
YLR448W	0.8228464	0.887341	0.80969631	0.66111821	0.614975112
YLR449W	0.77249647	0.86407141	0.51957999	0.44663409	0.359441586
YML001W	0.78605522	0.81145124	0.77421062	0.85494419	0.945018863
YML004C	0.03914253	0.10194132	0.01311275	0.01102317	0.023174804
YML008C	0.96743789	0.87219017	0.96316739	0.96187058	0.909514366
YML010W	0.39437451	0.57281671	0.84126731	0.65458357	0.658466022
YML017W	0.78588165	0.79669633	0.96740706	0.42533481	0.883963494
YML022W	0.07351222	0.07306739	0.05654079	0.07869998	0.072180995

YML025C	1	0.96590546	0.97662303	0.97367988	0.899197719
YML028W	0.11158152	0.12321639	0.08236869	0.10258701	0.122450314
YML035C	0.81483261	0.78308446	0.75009489	0.50034184	0.434940262
YML056C	0.98668446	0.87086285	0.74707958	0.78392602	0.777517939
YML057W	0.64473443	0.3558038	0.17290559	0.13164759	0.143632062
YML063W	0.94083975	0.89824268	0.87263614	0.75776075	0.743364278
YML069W	0.22249738	0.03180566	0.03827028	0.12516122	0
YML070W	0.46125453	0.3191509	0.02960622	0.05932436	0.17062136
YML072C	0.80097058	0.82230115	0.92685224	0.94533493	1
YML073C	0.7792404	0.86102271	0.84460112	0.60824152	0.627721141
YML074C	0.55086401	0.63774856	0.41049203	0.39666986	0.379808074
YML078W	0.0036415	0.00523538	0.00605557	0.01865068	0
YML085C	0.95146156	0.83944718	0.87148784	0.77997961	0.838718581
YML086C	1	0.86608625	0.92167854	0.92784091	1
YML092C	0.1816984	0.24880983	0.16612779	0.16530973	0.263517603
YML100W	0.717585	0.29039162	0.66658579	0.64967859	0.7473177
YML106W	0.00562745	0.0372809	0.00289529	0.03042213	0.053311792
YML115C	1	0.93437259	1	0.92410138	1
YML126C	0.09196889	0.06917262	0.05974607	0.07455075	0.112316789
YML127W	0.96249025	0.99745212	0.90319037	0.89725722	1
YMR004W	0.88686393	0.52838863	0.83604405	0.86584719	0.758416827
YMR012W	0.92784799	0.94800973	0.94894982	0.82279792	0.813991048
YMR024W	0.97992486	0.84337872	0.81464078	0.87583749	0.815939373
YMR027W	0.11759365	0.08324562	0.02064423	0.06456408	0.110077781
YMR033W	0.90502566	0.90014396	0.89563232	0.82728862	0.930182651
YMR038C	0	0.02516723	0.01252524	0	0
YMR039C	0.7276694	0.59278689	0.75124868	0.79257647	0.451961486

YMR049C	0.90094173	0.81696902	0.84432902	0.89958108	0.852989691
YMR072W	0.46036513	0.82347372	0.32117139	0.33034766	0.018189509
YMR079W	0.21139337	0.14625191	0.14428006	0.08307037	0.226704942
YMR080C	0.91085842	0.69451374	0.98591409	0.80924443	0.624036177
YMR083W	0.27860089	0.30016196	0.17116462	0.39571816	0.595899786
YMR086W	0.98871846	0.79928581	0.86889427	0.86704462	1
YMR092C	0.00626113	0.08167881	0	0.04877993	0
YMR093W	0.88566579	0.92555568	0.94479516	0.96483474	0.891261121
YMR099C	0.04037439	0.0498485	0.02487174	0.02722678	0.129154104
YMR105C	0.33234127	0.07655409	0.05769117	0.04407962	0.391425883
YMR108W	1	0.49801993	0.78944647	0.86606272	0.853423501
YMR116C	0.11131894	0.22237318	0.1135977	0.22958497	0.282177306
YMR120C	0.13807409	0.14910524	0.03453741	0.0675498	0.133206093
YMR121C	0.91175886	0.94957597	0.95923111	0.80007707	0.744325828
YMR125W	0.42865384	0.35179139	0.24041584	0.17364777	0.323165531
YMR128W	1	0.58262585	1	1	0.672079797
YMR131C	0.96665233	0.96982713	0.93251079	0.76006101	0.878606525
YMR142C	0.90673828	0.92041176	0.86606874	0.70793684	0.668373311
YMR146C	0.84835594	0.80955571	0.85744091	0.79684849	0.777965677
YMR169C	0.64216461	0.46437663	0.34685618	0.29766909	0.84705819
YMR170C	0.54885548	0.37104946	0.33538967	0.31199355	0
YMR186W	0.38048813	0.30087419	0.19429681	0.24381951	0.276647677
YMR188C	0.98860826	0.88664342	0.87816921	0.87482414	0.657350171
YMR189W	0.11050293	0.18969221	0.49813545	0.7808699	0.445581963
YMR203W	1	0.96814759	0.95875549	0.93614158	1
YMR205C	0.40911297	0.42164123	0.39428734	0.51029857	0.397677325
YMR212C	1	0.96086066	1	1	0.835206549

YMR217W	0.04467455	0.14619351	0.0183608	0.04167055	0.043653387
YMR226C	0.09835847	0.11619004	0.04241864	0.04612948	0.039977918
YMR229C	0.91440733	0.93760932	0.57686839	0.60997998	0.664452384
YMR235C	0.598135	0.1162989	0.06914406	0.11917837	0.270924405
YMR243C	1	1	1	1	0.977047639
YMR247C	0.84199976	1	1	0.91066364	0.936836025
YMR250W	0.13795537	0.24775957	0.09602146	0.0972461	0
YMR251W	0.22136447	0.14212949	0.06034809	0.03537988	0.807460991
YMR260C	0.0098791	0.15192217	0.09844981	0.36871051	0.338511931
YMR290C	0.92215278	0.7991884	0.89157191	0.92972942	0.873774003
YMR300C	0.10983195	0.25259454	0.18619543	0.30162237	0.276753154
YMR303C	0.63868167	0.51019287	0.21751935	0.22562079	0.323974088
YMR307W	0.63264214	0.61396862	0.81721713	0.91219553	0.930546539
YMR308C	1	0.8098825	0.64944908	0.62104755	0.922879824
YMR309C	0.92317349	0.76790886	0.85325229	0.81852188	0.823641296
YMR314W	0.25050071	0.17346341	0.15002828	0.23329579	0.059075238
YMR315W	0.17275985	0.07575042	0	0.0912577	0.290149623
YMR318C	0.0680599	0.15529973	0.01992772	0.01762646	0.012473653
YNL002C	1	0.8454341	0.92638679	0.89296322	0.867993953
YNL005C	0.98485771	0.98716603	0.88372122	0.96240194	0.675600433
YNL007C	0.7376594	0.5538893	0.79401717	0.71102803	0.712011779
YNL010W	0.32607127	0.12285032	0	0.01615632	0.176047032
YNL014W	0.78781345	0.42201642	0.43401641	0.57016457	0.230693856
YNL016W	0	0.18360146	0.00640813	0.11489866	0.403758786
YNL037C	0.51009964	0.69983322	0.38241141	0.35657051	0.389597397
YNL044W	0.98021076	0.83559152	0.77066996	0.92012105	0.646687177
YNL045W	0.6073666	0.10187795	0.1979197	0.13975046	0

YNL049C	0.95863235	0.94276407	0.93536061	0.95395344	1
YNL055C	0.98369372	0.97791413	0.99270572	0.87831693	0.964278322
YNL064C	0.98487203	0.77572461	0.81780873	0.73731857	0.768296931
YNL067W	0.82943913	0.93861263	0.92644206	0.73768468	0.754583213
YNL069C	0.89493915	0.92136933	0.91971912	0.6635607	0.678050049
YNL071W	0.94535522	0.82741877	0.95972685	0.87546764	0.943501584
YNL085W	0.2251687	0.1027679	0.65271424	0.72489965	0.759802002
YNL088W	0.9015809	0.87017859	0.92706778	0.87842108	0.766522424
YNL096C	0.84688843	0.85302776	0.85326445	0.69668799	0.737825658
YNL104C	0.12460964	0.14542034	0.04626263	0.08634011	0.513266539
YNL110C	1	0.93135977	0.80653056	0.79866774	0.762397786
YNL112W	0.57819224	0.92533307	0.86597614	0.72400956	0.623526806
YNL113W	1	0.84025232	0.75029363	0.79270258	0.844242059
YNL117W	0.21777336	0.16860195	0.10878538	0.07044702	0.128667618
YNL118C	1	0.76668511	0.74702904	0.93525417	1
YNL121C	0.99285456	0.88386811	0.85442272	0.87695259	0.989518924
YNL132W	0.96640089	0.98291493	0.99305965	0.94060326	0.890287569
YNL134C	0.0415766	0.07372955	0.00435121	0.02114662	0
YNL135C	0.15062239	0.13420088	0.059573	0.1324343	0.071470046
YNL137C	0.91008581	0.91782264	0.97654701	0.79815607	0.400419283
YNL138W	0.4404155	0.48950631	0.44974623	0.37120067	0.341928102
YNL139C	1	0.94185275	0.99353923	0.89581825	0.490165842
YNL168C	0.30305231	0.31261154	0.25278291	0	0.136369608
YNL178W	0.86620975	0.84052982	0.84594133	0.79048267	0.778887212
YNL182C	1	0.76160497	0.97022122	0.85555255	0.932073934
YNL200C	0.82502318	0.66690778	0.67943229	0.5253644	1
YNL207W	1	0.84853294	0.80198466	0.93828447	0.900263425

YNL209W	0.69107376	0.30912926	0.41738685	0.56310884	0.676907177
YNL220W	0.05350336	0.0641798	0.03168804	0.08582765	0.098096156
YNL232W	0.4289218	0.49364479	0.57839576	0.49375648	0.422583344
YNL239W	0.40713411	0.44625279	0.34362217	0.32518884	0.166805034
YNL241C	0.0981468	0.127465	0.10778489	0.16078673	0.251828141
YNL243W	0.77770624	0.38641656	0.74980672	0.64951492	0.826321875
YNL244C	0.37489317	0.14222814	0.29172029	0.36928321	0.325909454
YNL247W	0.20791032	0.14281938	0.03873807	0.05454828	0.031911614
YNL248C	0.98996568	0.95256397	0.91167459	0.89003837	0.809285301
YNL251C	0.84540669	0	0.42083314	0.08530354	0.271151298
YNL255C	0	0.66023413	0.14827672	0.93206948	0.927836998
YNL284C	1	0.91086404	1	0.59882216	0.942175305
YNL287W	0.96122156	0.83813983	0.85430791	0.63654701	0.828056181
YNL288W	0.98006245	0.89035842	0.98485258	0.97468446	0.95413574
YNL290W	1	0.93230424	0.8967398	0.95436528	0.5
YNL307C	0.57685264	0.21383878	0.33021385	0.43477399	0.445296202
YNL313C	0.44082404	0.43688206	0	0.25461068	0.145093156
YNL330C	1	0.84501255	0.72391314	0.78512492	0.804566734
YNL331C	0.15875752	0.27119991	0.07701121	0.27727087	1
YNR001C	0.21580264	0.22346629	0.21855024	0.27479492	0.353665438
YNR016C	0.87082769	0.66176336	0.51422059	0.28052473	0.499380846
YNR021W	1	0.94716348	1	0.99230223	1
YNR034W	0.07328353	0.02919743	0	0	0.14243617
YNR035C	0.69160843	0.45256855	0.5505959	0.36608859	0.63489305
YNR043W	0.0801186	0.09296476	0.04883072	0.03441209	0.011798033
YNR050C	0.19225175	0.07912445	0.05981179	0.05109631	0.097056829
YNR051C	0.98548001	0.82726834	0.87028412	0.86644386	0.669256765

YNR053C	0.83337468	0.94131789	0.96818987	0.9844954	0.945019244
YOL004W	0.89534497	0.95829315	0.91672703	0.68275699	0.550719319
YOL012C	0.89033803	0.93758726	0.83280721	0.48194208	0.482145633
YOL038W	0.33179649	0.45047509	0.29570928	0.22113195	0.264600254
YOL039W	0.86850353	0.82667019	0.82009521	0.77081752	0.656078274
YOL040C	0.87763497	0.95030285	0.81356557	0.66470677	0.591345571
YOL041C	1	0.96314232	0.90838889	0.86473962	0.819235148
YOL049W	0.08569132	0.08081993	0.01169952	0.02853613	0.081194127
YOL057W	0.09658968	0.05227922	0.01253715	0.08060161	0
YOL058W	0.08837242	0.10488249	0.02226772	0.04817172	0.100956988
YOL061W	0.93185714	0.71636513	0.51763128	0.66307508	0.591150127
YOL064C	0.03366271	0	0	0.00726617	0.036266945
YOL076W	0.97403206	0.91018725	0.98058658	0.91871046	0.967140296
YOL077C	0.94807933	0.89117206	0.93543164	0.87755265	0.864026587
YOL086C	0.44008324	0.37328889	0.25730905	0.33489981	0.525365085
YOL097C	0.09726701	0.09720617	0.20016987	0.15437948	0.246946087
YOL111C	0.84084912	0.94477845	0.81425477	0.63272482	0.734606819
YOL127W	0.86757294	0.92377592	0.85961735	0.78588048	0.736150131
YOL139C	0.58554257	0.29523324	0.43211076	0.52771266	0.532551975
YOL145C	0.79221716	0.49742146	0.7958556	0.71039247	0.700308328
YOL147C	0.9817966	0.96943739	1	0.93160272	0.948853417
YOL151W	0.03443293	0.0625212	0.00643967	0.05211228	0.038270532
YOR007C	0.37554829	0.17748559	0.10089338	0.21639083	0.104087099
YOR014W	1	0.96845294	0.85264897	0.6889686	1
YOR020C	0.42895943	0.24659895	0.24027106	0.17444902	0.112136031
YOR021C	0.09155679	0.08453536	0.01408383	0.09164071	0.034788074
YOR027W	0.03711807	0.06269242	0.05365604	0.09009543	0.055590313

YOR035C	0.87889251	0.55321483	0.61961305	0.44054699	0.833399309
YOR039W	0.84658375	0.11546956	0.95918114	0.85831736	0.852066087
YOR046C	0.21403016	0.24484617	0.17315301	0.31217992	0.302132648
YOR048C	1	0.92408561	0.88101206	0.87175816	0.811883348
YOR061W	0.72790337	0.9467407	0.85299441	0.80824112	0.772478001
YOR063W	0.90014622	0.92991081	0.87726047	0.74097086	0.672065321
YOR065W	1	0.88245776	1	1	1
YOR086C	1	0.97398984	0.95702434	0.95119099	1
YOR089C	0.92444312	0.91159107	0.73094392	0.82819601	0.917117724
YOR091W	1	1	0.95167639	0.78483721	0.898621345
YOR095C	0.14538958	0.26362396	0.07417276	0.019775	0.124127412
YOR096W	0.80849666	0.86018885	0.83218955	0.69814996	0.676993032
YOR099W	1	1	0.98359234	0.99154305	1
YOR109W	0.12423999	0.20339785	0.03021001	0.54039542	0.354322221
YOR116C	0.94444154	0.96788669	0.97128517	0.91427555	0.928985531
YOR117W	0.85487484	0.79035959	0.82290604	0.75740371	0.819541676
YOR120W	0.00422673	0.01250776	0	0.04637092	0
YOR122C	0.0158827	0.07322056	0	0.05151147	0.007026026
YOR128C	0.18937687	0.17783041	0.07725128	0.183132	0.301958834
YOR142W	0.07264136	0.05835768	0.05853159	0.04793842	0.129797243
YOR151C	0.25231082	0.48395018	0.32499469	0.35711989	0.389536807
YOR158W	1	0.99400933	1	0.88464414	0.859998838
YOR164C	0.98245204	0.87265375	0.94302237	0.77624894	0.865056459
YOR168W	0.08159658	0.16494331	0.10523157	0.14863451	0.147753065
YOR184W	0.33215328	0.20959235	0.11862183	0.17871776	0.201910962
YOR187W	0.28407186	0.06600253	0.05439749	0.29378561	0.039758435
YOR198C	0.82612278	0.64566289	0.78076352	0.72511425	0.637939931

YOR204W	0.91823079	0.91095897	0.84197763	0.75286028	0.696940691
YOR206W	1	0.95127821	0.99190916	0.94970876	0.854107087
YOR207C	1	0.93684548	0.93360961	0.90426378	0.762547724
YOR209C	0.03815462	0.02832189	0	0.02528924	0.027286222
YOR217W	0.93325748	0.95681297	0.94692468	0.84441629	0.547493788
YOR230W	0.14015563	0.16241063	0.05207118	0.06772616	0.49900253
YOR234C	0.83696051	0.91912077	0.86263556	0.70206631	0.664690858
YOR259C	0.8837363	0.85779258	0.84186881	0.89209025	0.8690657
YOR261C	0.76882717	0.49307455	0.75217666	0.46063607	0.650297212
YOR270C	0.87450785	0.9421736	0.91117884	0.97723701	0.987875882
YOR285W	0.16056747	0.09219685	0.04917034	0.06451629	1
YOR298C-A	0.98319839	0.44625496	0.63312093	0.8819891	0.540006283
YOR310C	0.93302808	0.89528423	0.91331287	0.86896621	0.893687167
YOR317W	0.98377718	0.93960107	0.9792624	0.92780148	0.956430445
YOR323C	0.08217558	0.19949789	0.00548079	0.09762848	0.018794131
YOR326W	1	0.86701267	1	0.82058913	0.719310935
YOR332W	0.56693107	0.42464469	0.26239014	0.38451279	0.257395133
YOR335C	0.47754398	0.22731194	0.0808847	0.20246686	0.361306089
YOR341W	0.96687123	0.83073477	0.83479248	0.77250763	0.801880984
YOR361C	0.93506993	0.81000153	0.90735081	0.82392274	0.79793206
YOR362C	0.29321436	0.4300355	0.33946202	0.30651549	0.264348227
YOR369C	0.35268801	0.29508185	0.35647051	0.42751688	0.435724079
YOR374W	0.22150789	0.2646653	0.19312336	0.19930072	0.269287186
YOR375C	0.07335442	0.26188825	0.06307823	0.11248056	0.151367635
YPL004C	0.72958701	0.41822827	0.30764979	0.2176709	0.350333326
YPL012W	1	1	0.98885063	0.94802319	0.989128441
YPL028W	0.08405093	0.15860348	0.05495846	0.08736929	0.12059433

YPL032C	0.96107169	0.83512212	0.93239904	1	0.799215836
YPL043W	0.77452759	0.8244435	0.79569224	0.79952698	0.683234899
YPL048W	0.3247588	0.37229613	0.31926078	0.38204907	0.282010907
YPL050C	1	0.91858335	1	0.98912597	1
YPL061W	0.14720455	0.13718295	0.06627886	0.13870041	0.163292111
YPL078C	0.95226892	0.90709378	0.98097797	1	1
YPL084W	0.87604572	0.75705016	0.63783583	0.60637863	0.709457652
YPL085W	1	1	1	0.83644446	1
YPL086C	0.9760164	0.90725107	0.91847335	0.91149294	0.844425867
YPL091W	0.20298884	0.23864555	0.09994747	0.13109106	0.06910304
YPL093W	0.95965751	0.93872368	0.97259199	0.94589129	0.852459131
YPL106C	0.316185	0.14730755	0.09771759	0.15724811	0.142484793
YPL111W	0.29762672	0.26402791	0.11402736	0.07578434	0.153538267
YPL112C	0.1315247	0.13760862	0.06591215	0.05321815	0.259879841
YPL117C	0.05481252	0.03951504	0.01935885	0.07069113	0.153146214
YPL119C	0.94923274	0.91941555	0.94208287	0.71904803	1
YPL120W	0.81723473	0.84667329	0.87559708	0.75479957	0.758662134
YPL125W	0.9623593	0.92705228	0.81791188	0.81548382	1
YPL127C	0.84107181	0.9220543	0.92728053	0.72924007	0.715619863
YPL128C	1	0.82120284	0.87340337	0.89593472	0.893853433
YPL129W	0.90237649	0.67080909	0.40932169	0.67113238	0.860622787
YPL131W	0.78152731	0.83617071	0.63636598	0.56023173	0.50321454
YPL143W	0.83159985	0.90185092	0.8583609	0.62993535	0.683004746
YPL154C	0.31099984	0.28067254	0.2908434	0.42992461	0.775158551
YPL160W	0.05666051	0.12160303	0.10726666	0.24133763	0.199464735
YPL169C	0.94223689	0.92306001	0.91376018	0.68560131	0.688140427
YPL190C	0.40595709	0.24099611	0.30178915	0.32595511	0.296320569

YPL195W	0.96871454	0.86044482	0.89576896	1	0.931316653
YPL198W	0.97564124	0.99152299	0.97081074	0.85944709	0.601954153
YPL203W	0.14147125	0.1220192	0.01480757	0.12523622	0.324782119
YPL204W	1	1	1	1	0.910658611
YPL210C	1	0.97286441	0.8037105	0.48044841	0.57085489
YPL211W	1	0.95843754	0.85221501	0.96354436	0.607430965
YPL218W	1	0.89778481	0.76440226	0.66999251	0.711452853
YPL225W	0.4144152	0.22340236	0.18114324	0.24664787	0.409446256
YPL226W	0.93471588	0.69613798	0.78483776	0.84438295	0.822653662
YPL231W	0.73286441	0.54328005	0.77170696	0.78327986	0.62517237
YPL235W	0.84491556	0.88235895	0.71271698	0.53307448	0.718222753
YPL237W	0.98480459	0.86139658	0.91042588	0.83737763	0.649961789
YPL240C	0.42999534	0.14508874	0.14501743	0.11460366	0.282257146
YPL243W	0.98148527	0.89131914	0.7534977	0.31916881	0.777571974
YPL249C-A	0.86051014	0.91208175	0.84715868	0.7031316	0.563248068
YPL260W	0.09308634	0.03200042	0.03794854	0.00568678	0.068616202
YPL262W	0.06232162	0.07201281	0.01913369	0.01827002	0.026577135
YPR010C	0.90993305	0.82796926	0.86464484	0.82782175	0.822277502
YPR034W	0.87197632	0.75828322	0.81296329	1	0.83267904
YPR035W	0.47818092	0.50369213	0.35249327	0.16254496	0.180246767
YPR036W	0.87217706	0.63149671	0.51623351	0.3045428	0.611952513
YPR041W	0.378658	0.35839752	0.53275127	0.64244722	0.697911626
YPR069C	0.06986233	0.02472381	0.00404129	0.06233748	0.056231134
YPR074C	0.04366419	0.07493752	0.02277663	0.0671611	0.085958245
YPR103W	0.27092379	0.15288713	0.12168943	0.31607996	0.651155449
YPR108W	0.88553737	0.66046168	0.5920964	0.52198732	0.886567096
YPR110C	0.7486533	0.79214331	0.79872356	0.71625032	0.827233837

YPR127W	0.06659295	0.09025964	0.0090648	0.03061548	0.333180652
YPR145W	0	0.25144294	0.0028097	0.02287835	0.031572025
YPR149W	0.93236717	0.91120273	0.97931327	0.95279964	1
YPR160W	0.50604561	0.34065821	0.0830964	0.11518094	0.33964476
YPR163C	0.09330474	0.15358073	0.07862925	0.10864224	0.108473372
YPR165W	1	0.94852901	0.81645112	0.98423074	0.960616669
YPR181C	0.3642556	0.36582825	0.44090103	0.53476306	0.581351248
YPR183W	1	0.89349427	0.99210167	0.97948896	0.973908862
YPR184W	0.2570253	0.30328907	0.17423076	0.02959258	0.689310132
YPR189W	1	0.97283761	0.86249065	0.92157417	0.876109358
YPR191W	0.73077152	0.58034569	0.5539562	0.42351289	0.545502388